EVOLUTION OF ATLANTIC DEEP-WATER CIRCULATION:

FROM THE GREENHOUSE TO THE ICEHOUSE

A Thesis

by

RACHAEL KATHLEEN VIA

Submitted to the Office of Graduate Studies of
Texas A&M University
in partial fulfillment of the requirements for the degree of

MASTER OF SCIENCE

August 2005

Major Subject: Oceanography

EVOLUTION OF ATLANTIC DEEP-WATER CIRCULATION:

FROM THE GREENHOUSE TO THE ICEHOUSE

A Thesis

by

RACHAEL KATHLEEN VIA

Submitted to the Office of Graduate Studies of
Texas A&M University
in partial fulfillment of the requirements for the degree of

MASTER OF SCIENCE

Approved by:

Chair of Committee,	Deborah J. Thomas
Committee Members,	Mitchell J. Malone
	Alejandro H. Orsi
	Niall C. Slowey
Head of Department,	Wilford D. Gardner

August 2005

Major Subject: Oceanography

ABSTRACT

Evolution of Atlantic Deep-Water Circulation:

From the Greenhouse to the Icehouse. (August 2005)

Rachael Kathleen Via, B.S., University of North Carolina at Chapel Hill

Chair of Advisory Committee: Dr. Deborah J. Thomas

To better understand how the evolution of Cenozoic deep-water circulation related to changes in global climate and ocean basin configuration, we generated Nd isotope records from Ocean Drilling Program sites in the southeastern Atlantic to track deep water mass composition through time. We used fossil fish debris from ODP Sites 1262-1264 (Leg 208), spanning present-day water depths of 2500-4750 m, to reconstruct the isotopic signature of deep waters over the past ~53 Ma. The data indicate an initial transition from relatively non-radiogenic values (ε_{Nd}=~-10) at 53 Ma to more radiogenic values (~-8.5) at ~32 Ma. From ~32 Ma to 3.85 Ma, the Nd signal becomes more non-radiogenic, ~-12.3 at the top of the record. Comparison of our data with Nd isotopic records derived from a North Atlantic Fe-Mn crust show similar non-radiogenic values (~-10.5) in the 53–32 Ma interval and a trend toward more non-radiogenic values beginning at ~20 Ma.

The data likely reflect an overall shift from a Southern Ocean deep water source to the ultimate incursion of deep waters from the North Atlantic. The non-radiogenic values at the base of the record reflect a Southern Ocean source of deep water. The shift toward more radiogenic values indicates an increased contribution of Pacific waters to the Southern Ocean source as the tectonic gateways changed after ~35-33 Ma. The subsequent trend toward more non-radiogenic Nd isotope values is approximately concurrent with the increase of benthic foraminiferal $\delta^{18}O$ values, based on comparison with a compilation of global data. Thus, changes in oceanic gateway configuration in

addition to overall cooling and the build-up of continental ice on Antarctica may have altered the Nd isotope character of Southern Ocean deep waters during the early Oligocene.

TABLE OF CONTENTS

Page

LIST OF FIGURES

LIST OF TABLES

1. INTRODUCTION

The flow of deep-water masses is one of the key controls on the distribution of heat, nutrients and dissolved gasses in the earth's oceans. As part of the meridional overturning, or thermohaline circulation, deep currents have demonstrated varying zones of formation and patterns of circulation throughout geologic time [e.g., *Pak and Miller*, 1992; *Brady et al*., 1998]. The formation of deep water occurs in discrete regions where air-sea interactions increase the density of surface waters and cause them to sink [e.g., *Tomczak and Godfrey*, 1994]. Global climatic and tectonic boundary conditions dictate the location of production areas for deep waters and their subsequent rate of overturning circulation at any given time. Climatic factors, such as the presence or lack of large ice sheets, meridional thermal gradients, and the balance of evaporation and precipitation, determine where and how deep waters form. Tectonic controls on circulation pertain to the morphology of ocean basins and locations of sills and gateways [*Hay*, 1995; *Crowley,* 1998]. As the size and shape of basins change through time, circulation patterns will adjust to maintain stability.

The present mode of meridional overturning circulation is characterized by deep-water formation in both the North Atlantic and the Southern Ocean (**Figure 1**). In the North Atlantic, brine rejection by the formation of sea-ice increases the salinity of already salty surface waters [*Colling*, 2001]. Combined with lower sea-surface temperatures, these waters become sufficiently dense to convect downwards. In the Southern Ocean, intense heat loss through ocean-atmosphere interaction and sea-ice formation renders surface waters cold enough to become dense and sink [*Colling*, 2001]. Waters formed in the North Atlantic move southward into the Antarctic Circumpolar Current where they mix with northward-flowing Antarctic Bottom Water (AABW), and their unity product fills the deep reservoirs of the Indian and Pacific Basins.

Early Cenozoic (~55 Ma) tectonic and climatic boundary conditions were significantly different from the present. Sea surface and deep-water oxygen isotope

---

This thesis follows the style of *Paleoceanography.*

records indicate that during this time, there was little to no large-scale continental ice and deep-ocean waters were warmer than today [*Zachos et al*., 2001]. With warm bottom and surface waters, the surface-to-deep thermal gradient was comparatively small, and due to the relatively warmer high latitudes, the equator-to-pole thermal gradient was small as well. A weak meridional thermal gradient in the oceans is a key factor in the maintenance of overall warmer climates of the Late Cretaceous and Early Cenozoic [*Brady et al*., 1998]. In light of these climatic differences, it follows that the nature of thermohaline circulation in the Early Cenozoic would have been fundamentally different from today.

Deep waters were not able to form in the North Atlantic during the early Cenozoic because the northern North Atlantic basins (the Greenland, Norwegian and Labrador Seas) had not yet fully formed (**Figure 2**). Additionally, prior to the opening of theses basins, deep water potentially formed in the Arctic would have been restricted to the North Polar Basin. The Drake Passage and the Tasman Sea were not open, effectively compartmentalizing the Atlantic and Pacific basins at high southern latitudes. The Caribbean gateway and Tethys Ocean, however, were still open, allowing for exchange between the Atlantic and Pacific at lower latitudes. Until the formation of the Panama Isthmus (~4 Ma; e.g., *Burton et al*. [1997]), the Gulf Stream would not be deflected poleward, thereby reducing the flux of saline water to higher northern latitudes and thus limiting the ability to form deep waters by the present mechanism. Given these climatic and tectonic constraints, model studies [*Brady et al*., 1998] and proxy data [*Thomas et al*., 2003] have indicated the Southern Ocean likely was the dominant region of deep-water formation for a large portion of the Cenozoic. As global climate cooled and tectonic gateways changed through the past ~65 million years (m.y.), this mode of deep-ocean circulation gradually evolved into the modern mode, characterized by both Southern Ocean and North Atlantic deep water sources of roughly equal strengths [*Orsi et al*., 2001; *Orsi et al*., 2002].

As source regions for deep-water change, so will the fluxes of heat and freshwater throughout the ocean basin. Cold, deep waters forming in the polar regions

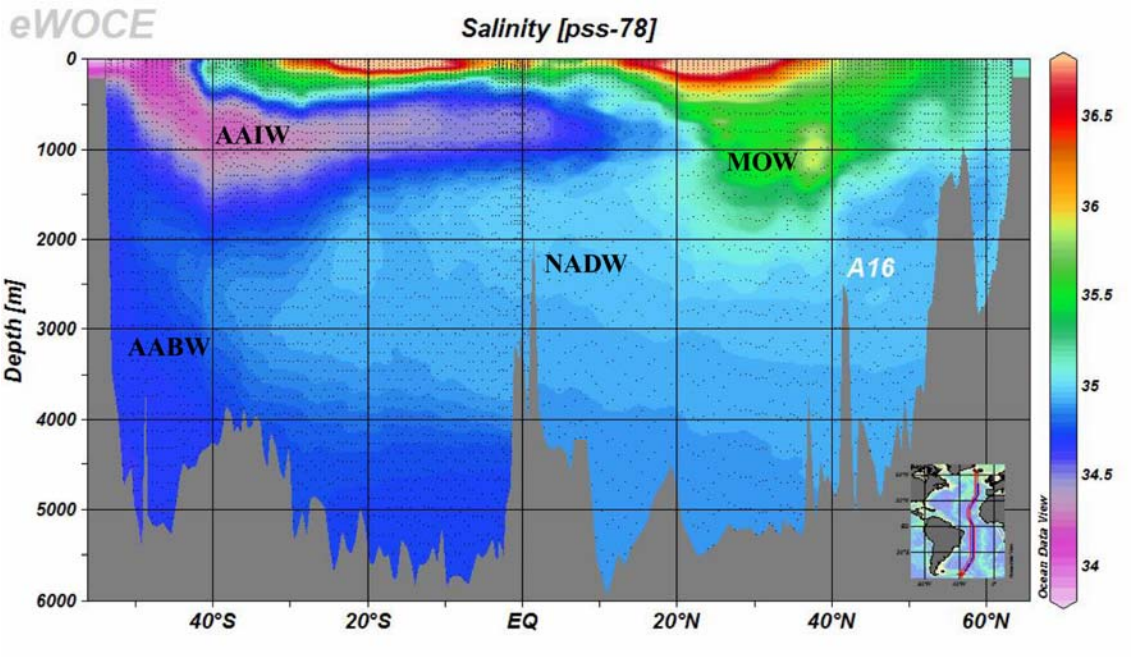

Figure 1. Vertical structure of the Atlantic Ocean based on salinity. AAIW: Antarctic Intermediate Water; NADW: North Atlantic Deep Water; MOW: Mediterranean Outflow Water. *World Ocean Circulation Experiment.*

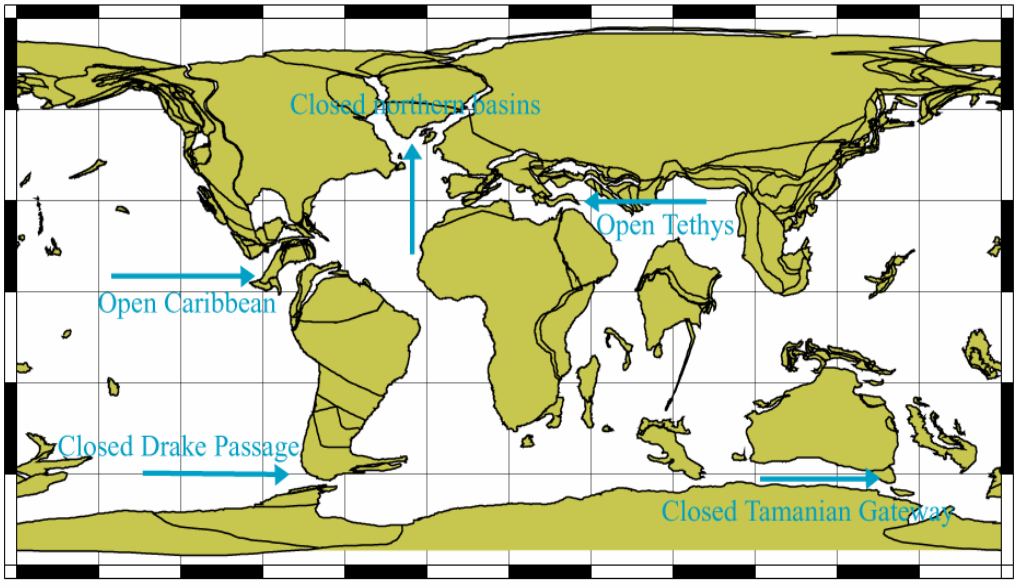

Figure 2. 55 Ma tectonic reconstruction. Note: does not include paleo-sea level. *Ocean Drilling Stratigraphic Network.*

are transported to lower latitudes by way of deep western boundary currents, which eventually upwell to the surface layer within the interior [*Stommel and Arons,* 1960]. If deep waters were to form in equatorial regions, the upwelling of warm saline bottom waters (WSBW) at high latitudes would bring more heat poleward and likely decrease the earth's ability to maintain large-scale ice caps. This mechanism has been used to explain the warm climates and bottom waters (up to 15° C) of the Late Cretaceous (70 Ma; *Brass et al*. [1982], *Hay* [1995]), but has been the source of some debate [*Brady et al*., 1998; *DeConto et al*, 2000].

Global Cenozoic deep-water temperatures exhibit a first-order cooling trend throughout the entire era, from approximately 10°C in the early Paleocene (65 Ma) to about -2° C presently [e.g., *Zachos et al*., 2001]. The ability to identify regions of deep-water formation and to characterize changes in their strengths as well as in the downstream deep-circulation patterns through time enables us to better understand why and how the oceans will react to changing tectonic and climatic boundary conditions. Here, we have used the neodymium isotopic composition of fossil fish debris as a proxy for tracking changes in deep-water composition of the southeastern Atlantic Ocean during a time of overall cooling, specifically, through the past ~53 Ma.

2. BACKGROUND

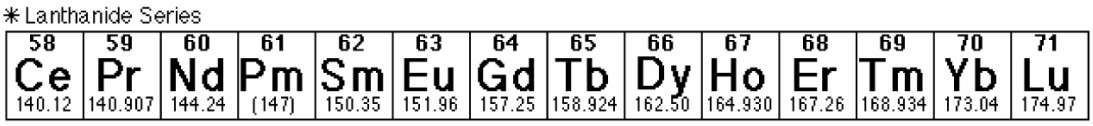

Figure 3. The Lanthanide series. Ce through Eu (along with La) are considered light rare earth elements.

2.1 Nd isotope geochemistry

Neodymium, a rare earth element (REE; **Figure 3**), has seven naturally occurring isotopes: ^{142}Nd, ^{143}Nd, ^{144}Nd, ^{145}Nd, ^{146}Nd, ^{148}Nd and ^{150}Nd. The ratio of radiogenic ^{143}Nd to stable ^{144}Nd is most commonly used in geochemical investigations. The ^{143}Nd nuclide is produced by α-decay of ^{147}Sm, which has a half-life of 1.06 x 10^{11} years. Differences in the ^{143}Nd/^{144}Nd ratio of rocks arise from age differences, but also through fractionation of Nd and Sm. Continental rocks, although they tend to be old, were extracted relatively early from the mantle and so have low Sm/Nd, and in turn, low ^{143}Nd/^{144}Nd. Oceanic basalts that originate from a depleted mantle inherit relatively high Sm/Nd, and thus have high ^{143}Nd/^{144}Nd. The typical Sm/Nd value for granite, a cratonic rock, is 0.188, whereas the typical Sm/Nd value for a mid-ocean ridge basalt is 0.320 [*Faure*, 1986]. Due to the long half-life of ^{147}Sm and the small range of Sm/Nd, changes in the ^{143}Nd/^{144}Nd ratio are relatively small. Nd isotope data are expressed in epsilon notation, ε_{Nd}, which normalizes the ^{143}Nd/^{144}Nd ratio to the chondritic uniform reservoir (CHUR):

$$\boldsymbol{\varepsilon_{Nd} = \{[(^{143}Nd/^{144}Nd}_{\text{ sample}})/ \mathbf{I^0_{CHUR}}] - 1\} \times 10^4$$

[*DePaulo and Wasserburg*, 1976],

where I^0_{CHUR} is the present ^{143}Nd/^{144}Nd ratio of CHUR, equal to 0.512638. To correct for in situ production of ^{143}Nd in a mineral, we define $\varepsilon_{Nd}(t)$:

$$\boldsymbol{\varepsilon_{Nd}(t) = \{[(^{143}Nd/^{144}Nd)_i / I^t_{CHUR}] - 1\} \times 10^4}$$

[*DePaulo and Wasserburg*, 1976],

where $(^{143}Nd/^{144}Nd)_i$ is the initial $^{143}Nd/^{144}Nd$ ratio of the rock and I^t_{CHUR} is the ratio of CHUR at a given time *t* in the past [*Faure*, 1986].

Both Sm and Nd are highly immobile and are not fractionated significantly from each other as crustal rocks weather. A study of the suspended sediment load of 31 rivers in different regions shows that the $^{147}Sm/^{143}Nd$ composition of a river is essentially equal to that of the upper crust it drains [*Goldstein and Jacobsen,* 1988]. This chemical weathering and drainage of subaerally-exposed rocks is the principal source of Nd to the oceans [*Elderfield and Greaves*, 1982; *Goldstein and Jacobsen*, 1988].

Although hydrothermalism is a significant source of many dissolved minor and trace elements to seawater, it is not a major contributor of Nd to the water column. Mid-ocean ridge basalts (MORBs) are significantly depleted of light rare earth elements (LREEs) compared to seawater, implying that alteration of oceanic crust would have a negligible effect on the ε_{Nd} signature of bottom waters [*Michard et al.,* 1983; *Piepgras and Wasserburg,* 1984]. In contrast, hydrothermal solutions are enriched in LREEs relative to seawater, though their contribution of Nd to seawater is orders of magnitude less than that of continental derived components [*Michard et al.,* 1983]. *Halliday et al*. [1992] calculated extremely short residence times (<1 year) for Nd in hydrothermal solutions, concluding that Nd is scavenged sufficiently rapidly not to affect the dissolved ε_{Nd} signature of the water column. Metalliferous sediments have REE signatures similar to hydrothermal solutions, indicating that their precipitation is a sink for hydrothermal Nd.

Eolian inputs are also negligible to the Nd concentration of seawater. Wind-blown particles from the Asian continent are the only significant source of silicate sediments to the North Pacific. Average ε_{Nd} values for Chinese loess are ~-10 [*Jones et al*., 1994], whereas Pacific waters are far more radiogenic (~-4, *Piepgras et al.* [1979]). The work by *Jones et al*. [1994] established that Nd is not significantly leached from suspended loess and thus not an appreciable source of Nd to the water column.

2.2 Nd as a tracer of ocean circulation

Weathering and runoff primarily deliver Nd to oceanic surface waters. Intermediate- and deep-water formation results in a water mass with the surface-water Nd signal of the formation region. More negative seawater ε_{Nd} values indicate weathering and drainage of non-radiogenic source regions (where concentrations of Sm are the lowest), and less negative ε_{Nd} values indicate drainage of more radiogenic source regions (higher Sm concentrations). Currently, the most negative seawater values are found in the Labrador Sea (ε_{Nd} = -28 surface, -14 deep; **Figure 4**); the non-radiogenic signal reflects drainage of the Precambrian rocks of the Canadian craton. In contrast, deep waters in the North Pacific have less negative values (ε_{Nd} =~-4 or -5), due to the weathering of younger circum-Pacific arc terranes. The inter- and intra-basinal differences of seawater ε_{Nd} (**Figure 4**) suggest that the residence time of Nd in the ocean is less than the deep global mixing time of the ocean (~1500 years; *Broecker et al*. [1960]). Current estimates of the residence time of Nd in the ocean are on the order of a few hundreds of years [*Tachikawa et al*., 1999].

The ε_{Nd} signature of a given water mass evolves during advection away from the source due to water mass mixing. For example, the typical present-day ε_{Nd} value for NADW in the Northern Hemisphere is between -13 and -14. These values are obtained as a result of the mixing of highly non-radiogenic Labrador Sea Water (ε_{Nd} = -28) with less non-radiogenic waters from the Greenland and Norwegian Seas (ε_{Nd} = ~-8 to -10).

Changes in weathering may also contribute to changes in the ε_{Nd} value of a water mass. A change in NADW ε_{Nd} could result from two factors. First, it could indicate a change in the balance of relative contributions from the Labrador Sea or Greenland/Norwegian Sea components, which in turn implies an alteration in the northern Atlantic circulation. Second, the material being weathered into the source region may also change. As glaciers grow and retreat, the change in the balance of chemical versus physical weathering can alter the minerals that are weathered, resulting in drainage of a different $^{143}Nd/^{144}Nd$ signal.

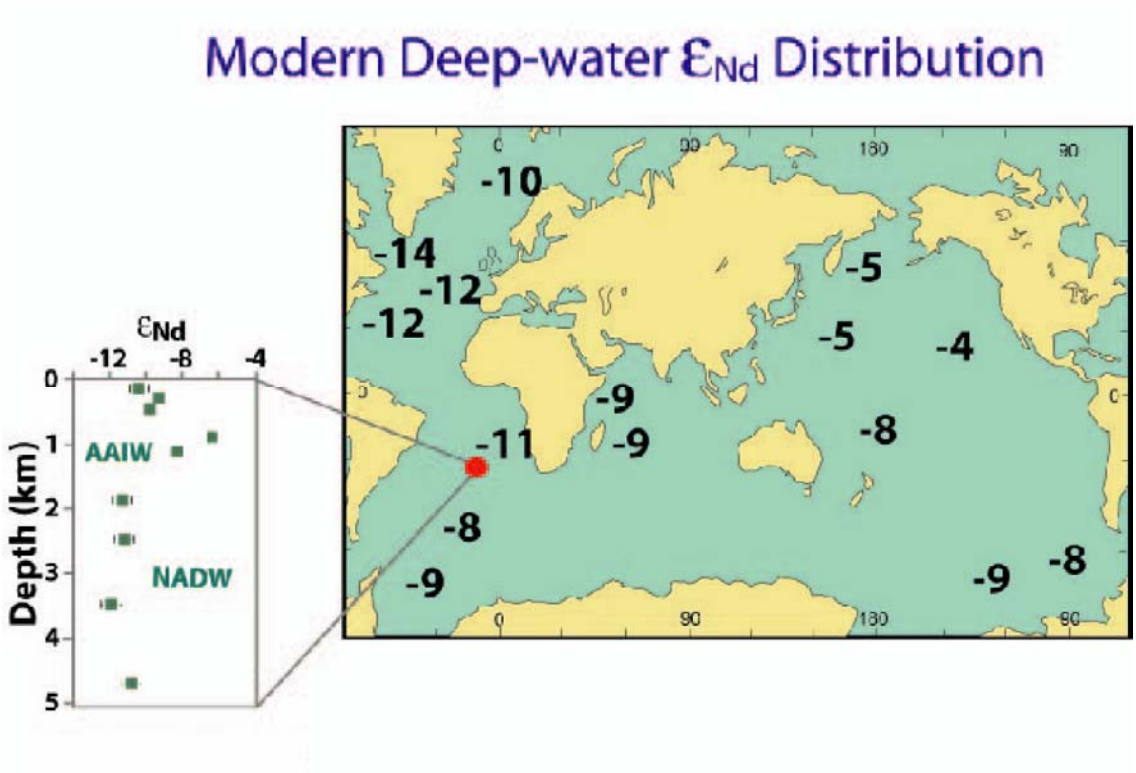

Figure 4. Compilation of modern deep-water ε_{Nd}, after *Jones et al.* [1994]. Inset: Water column ε_{Nd} profile after *Jeandel* [1993], showing layering of intermediate- and deep-water masses.

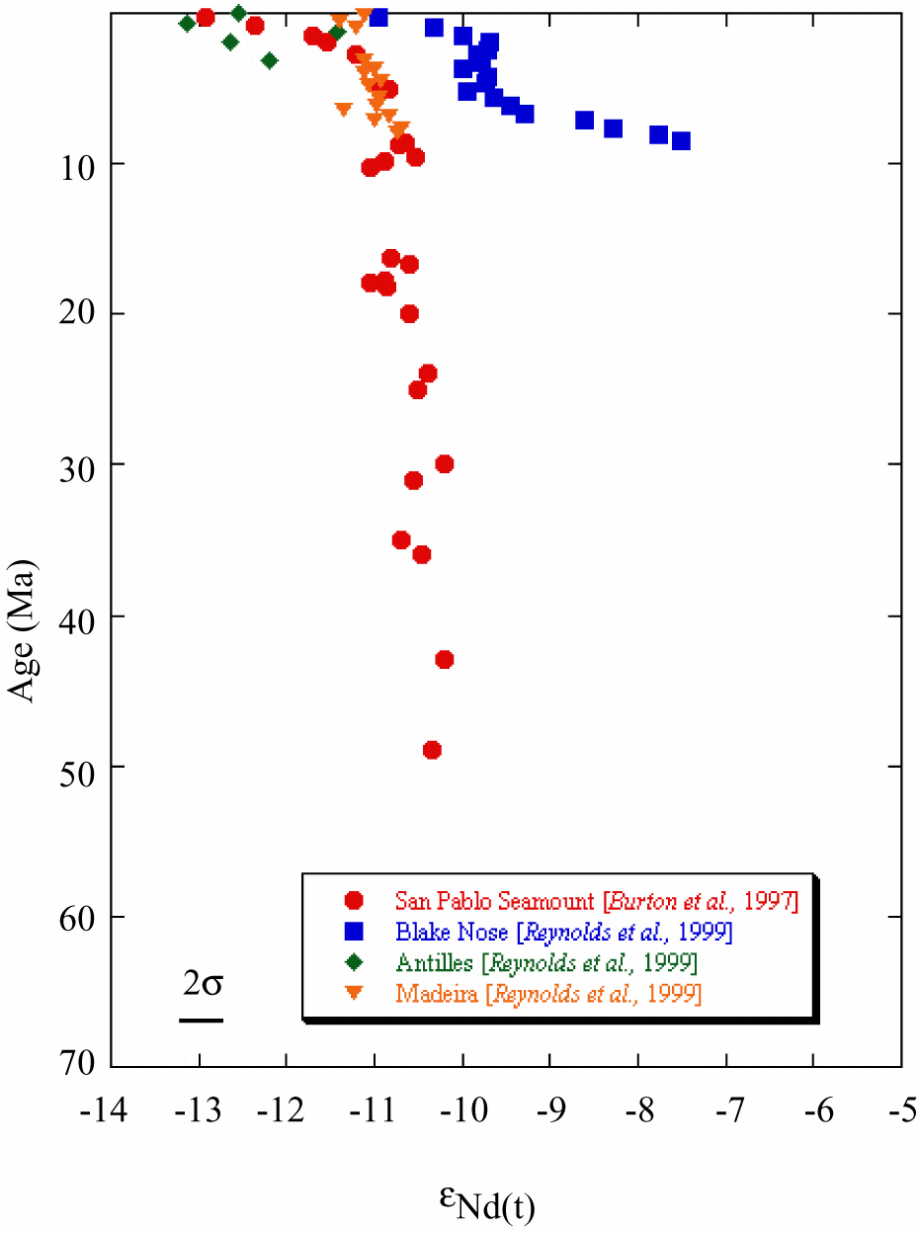

Figure 5. Atlantic ε_{Nd} records constructed from various Fe-Mn crusts.

Although the ε_{Nd} signal delivered to a water mass may change, it is still interpreted as ultimately reflecting the water's provenance and mixing history. To extend the previous example, NADW retains its original non-radiogenic fingerprint from its source region as it travels to the Southern Hemisphere. By the time it reaches Walvis Ridge, due to the advection of more radiogenic surface waters, NADW has an ε_{Nd} signature between ~-11 to -12. Though the ε_{Nd} signal of a water mass evolves during transit, it is still a conservative property and therefore a robust tracer of deep-ocean circulation.

2.3 Construction of paleo-Nd isotope records

Several phases record the Nd isotopic composition of deep-water masses. Ferromanganese crusts and nodules precipitate directly from seawater, recording the ε_{Nd} of the water in which they formed. Crust records provide a low-resolution framework for tracking changes in Atlantic thermohaline circulation [*O'Nions et al*, 1998; *Abouchami et al*, 1999; *Burton et al*., 1999; *Reynolds et al*., 1999; *Frank et al*., 2002; *van de Flierdt et al*., 2004]. A crust dredged from the San Pablo seamount (**Figure 5**) in the northwestern Atlantic (1850 m water depth) indicates non-radiogenic deep water through most of the Cenozoic. This record, along with three other crusts from the Blake Plateau (~850 m), the Antilles Desirade Seamount (~2000 m), and the Maderia Abyssal Plain (4867 m) [*Reynolds et al.,* 1999], displays a trend toward more non-radiogenic values since ~5 Ma.

Foraminiferal calcite [*Vance and Burton*, 1999; *Vance et al*., 2004] as well as Fe-Mn coatings on foraminifera tests [*Palmer and Elderfield*, 1986] have been shown to record a seawater ε_{Nd} signal as well. Foraminiferal records, however, are limited in their extent due to the dissolution of carbonate below the calcite compensation depth (CCD). Authigenic Fe-Mn oxides disseminated in sediments also record the REE composition of seawater at the seafloor [*Rutberg et al*., 2000; *Piotrowski et al*., 2004].

Biogenic apatite ($Ca_5(PO_4)_3(OH,F,Cl)$) in deep-sea sediments contains high concentrations of Nd (~100-1000 ppm; *Staudigel et al*. [1985], *Grandjean et al*. [1987],

Martin and Scher [2004]). Apatite is resistant to dissolution in deep waters and is ubiquitous in the Cenozoic marine geologic record, both spatially and through time. The teeth and bones of living fish do not contain any rare earth elements, thus where the fish lived and swam is does not affect the REE signal in fossil teeth and bones. Fish debris acquires an enhanced Nd concentration after deposition on the sea floor but while still in contact with the overlying water [e.g. *Reynard et al*., 1999; *Martin and Scher*, 2004]. Typical Nd concentrations in fish teeth are as high as 1000 ppm, representing a five-order of magnitude increase over the Nd composition of seawater (~10s of pmol, *Elderfield and Greaves* [1982]). Nd is "preconcentrated" by scavenging and re-release during the oxidation of organic matter at the sediment-water interface. Early diagenetic recrystallization then incorporates REEs into the phosphate lattice.

Once the fish debris is buried, its isotopic composition is not altered. Several lines of evidence suggest that REE exchange between sedimentary phases and pore waters is low. *Henderson and Burton* [1999] calculated diffusion rates for Nd in Fe-Mn crusts and found that they were low, indicating that Nd is highly immobile in marine sediments. Though pore water Nd concentrations are enhanced relative to seawater (~10-1000 pmol/L; *Haley et al*. [2004]), they are far lower than concentrations in the fish debris (~100-1000 ppm) and thus will not have any noticeable affects to the $^{143}Nd/^{144}Nd$ ratio. *Martin and Scher* [2004] supported this by finding that measured Nd concentrations in samples from the same site but of ages nearly 15 million years apart have similar concentrations. These studies show that there is no continued overprinting of Nd after burial. Therefore the $\varepsilon_{Nd}(t)$ record of fossil fish debris is a reliable archive for temporal variations in deep and bottom waters bathing a given region.

2.4 Geologic setting of ODP Sites 1262-4

Walvis Ridge, located in the southeastern Atlantic (**Figure 6**), is ideally situated to track changes in deep-water contributions from both the Southern Ocean and the North Atlantic. It blocks the northward flow of AABW in the eastern portion of the South Atlantic, and is also positioned near where present-day NADW initially merges into the Antarctic Circumpolar Current (ACC) [*Tomczak and Godfrey,* 1994]. Walvis Ridge formed in the late Campanian and early Maastrichtian (71-69 Ma; *Moore, Rabinowitz, et al*., [1984]) by hotspot activity associated with the widening of the South Atlantic basins [*Rabinowitz and LeBrecque*, 1979; *Moore, Rabinowitz, et al*., 1984]. Walvis Ridge likely subsided ~1.1 km during the past 65 Ma [*Moore, Rabinowitz, et al*., 1984]. The ridge trends northeast to southwest, extending approximately 2100 km from the continental margin of Namibia (~20°S) to the active volcanic islands of Tristan de Cunha and Gough, adjacent to the Mid-Atlantic Ridge (~40°S). Presently, the Walvis Ridge separates the Angola Basin to the north from the Cape Basin to the south.

The sedimentary deposits on Walvis Ridge are calcareous chalks and oozes, Campanian (70-80 Ma) to Holocene (0 Ma) in age [*Zachos, Kroon, Blum, et al*., 2004; *Moore, Rabinowitz, et al*., 1984]. These deposits range in thicknesses from 300-600 m. Sedimentation rates vary from ~8-13 meters per million years (m/m.y.) in the Late Cretaceous and early Paleogene to ~1-5 m/m.y. in condensed intervals in the Neogene [*Zachos, Kroon, Blum, et al*., 2004]. The ridge is also characterized by turbidite sequences and slumping in some Neogene intervals and in the upper Paleocene at DSDP Site 529 (**Figure 7;** *Zachos, Kroon, Blum, et al*. [2004]; *Moore, Rabinowitz, et al*., [1984]).

A depth transect of sites was drilled along the Walvis Ridge by Ocean Drilling Program Leg 208 (**Figure 7**) in 2003 to investigate the extreme climatic events of the Early Cenozoic, such as the Cretaceous/Tertiary boundary, the Paleocene/Eocene Thermal Maximum and the early Oligocene Glacial Maximum. One of the primary

scientific objectives of the leg was to reconstruct the evolution of deep-water composition, thus this study is directly related to the original drilling goals.

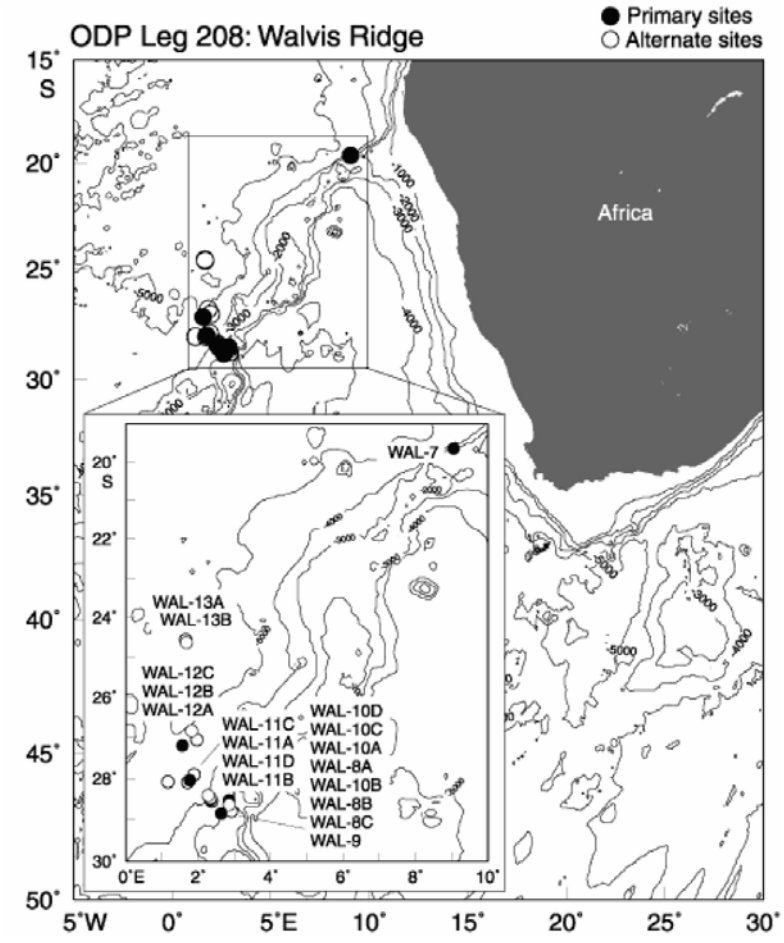

Figure 6. Location of Walvis Ridge in SE Atlantic. From *Zachos, Kroon, Blum et al.* [2003].

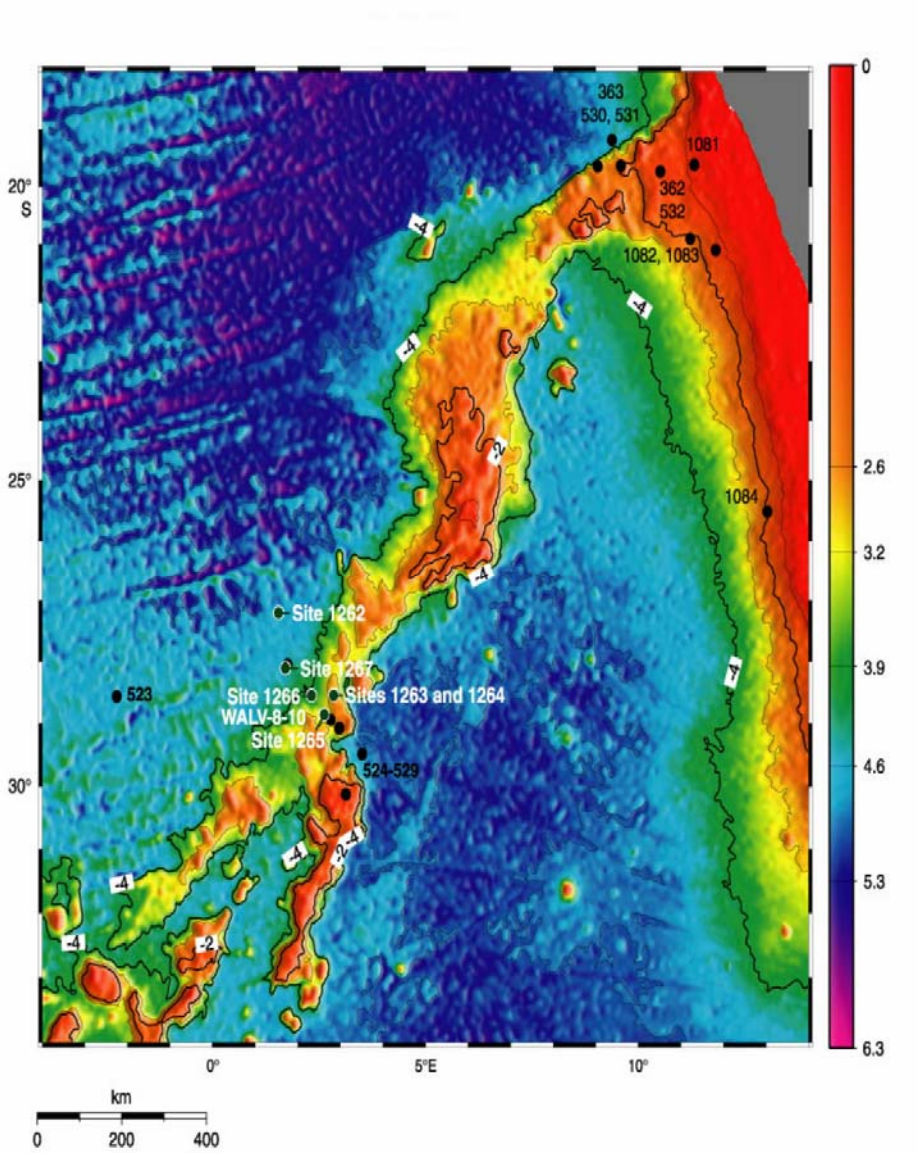

Figure 7. Bathymetric profile in km below sea level. From *Zachos, Kroon, Blum et al.* [2003].

3. SAMPLES AND METHODS

3.1 Samples

We analyzed samples from Sites 1262 (27°11.15′S, 1°34.62′E), 1263 (28°31.98′S, 02°46.77′E), and 1264 (28°31.95′S, 2°50.73′E), located sequentially down the flank of Walvis Ridge at present day water depths of 2505 m, 2717 m and 4755 m (**Figure 7**). Paleodepths ranged from ~1500 m to ~3500 m in the earlier part of the record (55 Ma; **Figure 8**). The sampling interval spans the past ~53 Ma. Initial samples were collected at a frequency of one per core (a resolution of ~1 m.y.). In addition, higher-resolution samples from Hole 1262A were collected at a frequency of one per section for a resolution of ~150 ky. The strategy of analyzing samples from Sites 1262-1264 was to generate a profile of the vertical structure of the water column through time.

3.2 Age model

The ages assigned to the samples are based on shipboard calcareous nannofossil data [*Zachos, Kroon, Blum, et al*., 2004]. Biostratigraphic datums were based on the timescales of *Cande and Kent* [1995] for the Late Cretaceous to early Oligocene, H. Pälike et al. [pers. comm., 2003] for the late Oligocene and *Lourens et al.* [2004] for the Neogene. Linear sedimentation rates were calculated between datums to yield a numeric age for each sample (**Table 1**).

3.3 Analytical methods

Samples were dispersed in a dilute sodium metaphospate solution and washed with 18.2 MΩ Milli-Q water through a 63 μm sieve. Fish debris was hand-picked using a microscope. Teeth were cleaned using a strong reductive/oxidative cleaning protocol to remove the oxide coating and any residual organic material (modified from *Boyle*

[1981], *Boyle and Keigwin* [1985]), and dissolved in 2N HNO_3. The REE suite of the teeth was isolated by cation exchange chemistry, from which Nd was then isolated by chromatographic separation. The complete analytical procedure is listed in Appendix A. Samples were analyzed as NdO^+ with a monitor beam ($^{144}Nd^{16}O$) of ~500 mV on a GV Sector 54 thermal ionization mass spectrometer (TIMS) at the University of North Carolina at Chapel Hill. External reproducibility based on analysis of the $J_{Nd}i$ standard is +/- 0.14 epsilon units (n = 29). The blank was 15 pg and considered negligible.

Table 1. Biostratigraphic datums for Holes 1262A, 1263A and 1264A. From *Zachos, Kroon, Blum, et al*. [2004].

Hole	datum	average age	mcd
1262A	*Gephyrocapsa parallela*	1.005	6.05
	Large Gephyrocapsa	1.24	8.74
	Medium Gephyrocapsa spp.	1.7	13.49
	Zone CN13a assemblage	1.75	16.01
	Zone CN12aB assemblage	3.245	17.22
	Zone CN10c assemblage	4.805	35.72
	Ericsonia formosa	32.9	75.29
	Discoaster saipanensis	34	78.12
	Discoaster barbadiensis	34.2	78.12
	Tribrachiatus orthostylus	51	96.91
	Discoaster lodoensis	52.4	107.67
	Discoaster multiradiatus	53	113.25
	Tribrachiatus orthostylus	53.4	118.25
	Fasciculithus spp.	54.1	137.04
	Discoaster multiradiatus	56.2	151.93
	Heliolithus riedelii	57.3	168.83
	Discoaster mohleri	57.5	168.83
	Heliolithus kleinpellii	58.2	175.18
	Sphenolithus anarrhopus	58.4	175.18
1263A	*Discoaster pentaradiatus*	2.52	2.29
	Discoaster surculus	2.63	2.29
	Amaurolithus spp.	4.56	12.07
	CN9a/NN11 assemblage	7.835	26.33
	Sphenolithus ciperoensis	27.55	48.00
	Sphenolithus distentus	30.32	56.35
	Reticulofenestra umbilicus >14 µm	31.7	75.91

Table 1. (continued)

	Isthmolithus recurvus	32.7	85.52
	Ericsonia formosa	32.9	85.52
	Ericsonia obruta increase	33.7	94.49
	Discoaster saipanensis	34	103.87
	Isthmolithus recurvus	36.6	116.30
	Dictyococcites bisectus	38.5	135.45
	Dictyococcites scrippsae	40.3	138.74
	Nannotetrina spp.	42.3	155.75
	Reticulofenestra umbilicus >14 µm	42.5	159.14
	Nannotetrina spp.	47.8	213.54
	Discoaster lodoensis	48	215.04
	Rhabdosphaera inflata	48.5	222.69
	Discoaster sublodoensis	49.3	228.68
	Tribrachiatus orthostylus	51	247.15
	Discoaster lodoensis	52.4	275.58
	Toweius crassus	51.5	281.23
	Discoaster multiradiatus	53	286.42
	Sphenolithus radians	53.3	287.92
	Tribrachiatus orthostylus	53.4	295.30
	Discoaster diastypus	53.9	328.78
	Discoaster multiradiatus	56.2	357.50
	Discoaster nobilis	56.5	366.34
	Heliolithus riedelii	57.3	388.15
	Discoaster mohleri	57.5	389.65
	Heliolithus kleinpellii	58.2	400.23
	Sphenolithus anarrhopus	58.4	400.23
	Large Gephyrocapsa spp.	1.24	6.16
1264A	*Large Gephyrocapsa spp.*	1.58	8.16
	Calcidiscus macintyrei	1.67	9.16
	Medium Gephyrocapsa spp.	1.69	9.66
	Discoaster brouweri and D. triradiatus	1.96	11.16
	Discoaster pentaradiatus	2.52	15.53
	Discoaster surculus	2.63	16.23
	Discoaster tamalis	2.83	17.73
	Sphenolithus spp.	3.66	28.89
	Reticulofenestra pseudoumbilicus	3.82	30.39
	Amaurolithus spp.	4.56	34.18
	Ceratolithus acutus	5.37	76.54
	Nicklithus amplificus (top)	6.00	77.04
	Nicklithus amplificus (bottom)	6.84	82.82
	Amaurolithus primus	7.39	110.64
	Paracme Reticulofenestra pseudoumbilicus	8.79	121.36

Table 1. (continued)

Discoaster hamatus	9.63	141.69
Catinaster calyculus	9.64	144.09
Discoaster neohamatus	8.45	146.39
Discoaster bellus gr. (= B D. hamatus)	10.48	148.59
Catinaster coalitus	10.79	161.34
Coccolithus miopelagicus	11.02	169.34
Discoaster kugleri	11.6	171.97
Discoaster kugleri	11.88	171.97
Triquetrorhabdulus rugosus	12.81	184.42
Sphenolithus heteromorphus	13.55	186.62
Discoaster signus gr.	15.6	198.11
Acme Discoaster deflandrei	15.6	198.11
Sphenolithus heteromorphus	17.76	210.09
Sphenolithus belemnos	17.89	210.09
Sphenolithus belemnos	18.92	216.15
Sphenolithus delphix	23.07	257.65
Sphenolithus delphix	23.33	260.98
Sphenolithus ciperoensis	24.23	262.64
Sphenolithus ciperoensis	27.55	282.11
Sphenolithus distentus	30.32	306.08

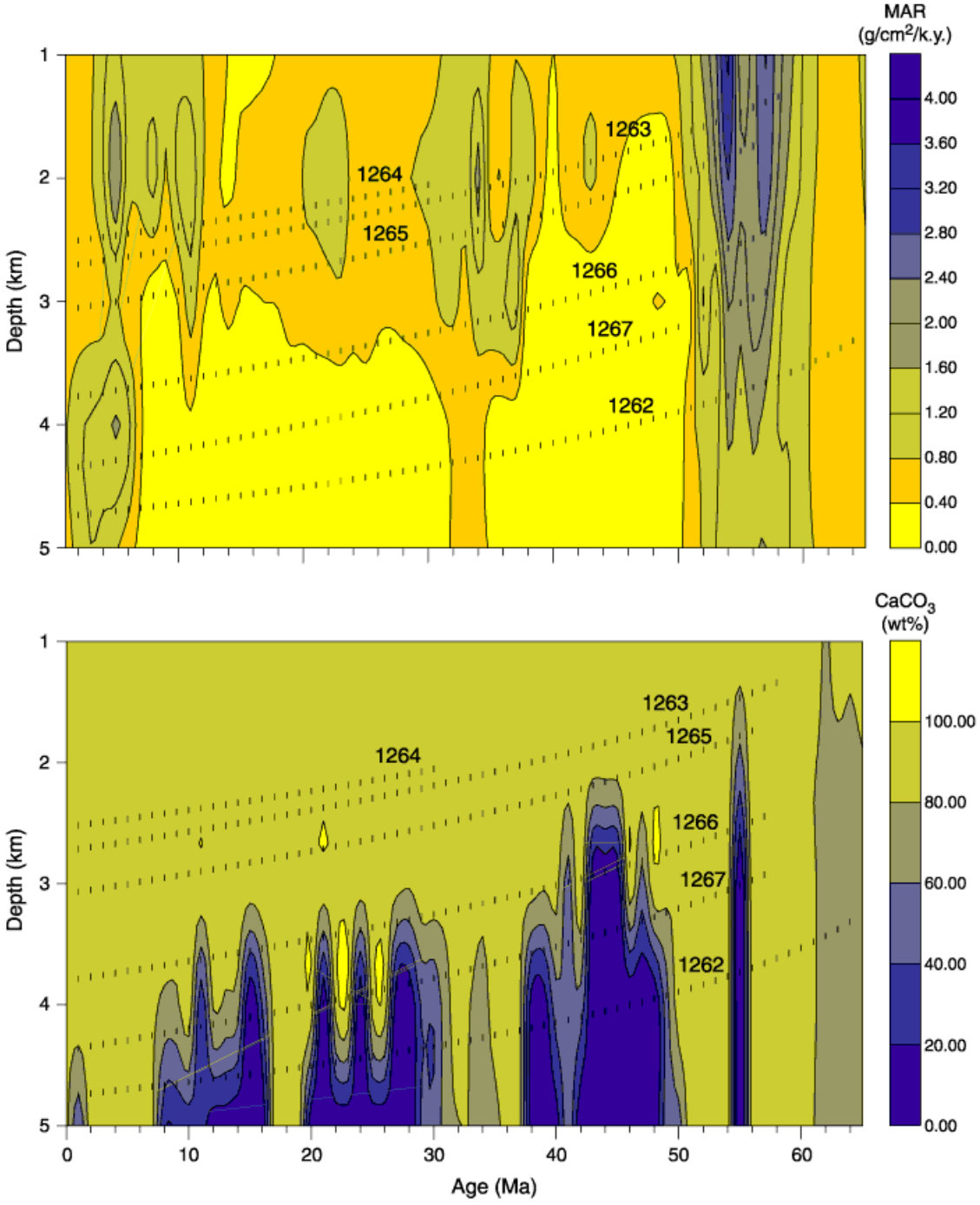

Figure 8. Subsidence curves, mass accumulation rates and carbonate content plots for Leg 208. From *Zachos, Kroon, Blum, et al*. [2004].

4. RESULTS

Samples from Site 1262 range in age from 58.4 to 4.3 Ma and span 30.48 to 176.6 m composite depth (mcd) (**Table 2**). The base of the record (**Figure 9**) shows $\varepsilon_{Nd}(t)$ values of ~-10 to -9. A trend towards more radiogenic values (up to >-6) begins around 50.24 Ma (91.71 mcd), with a return to non-radiogenic values (~-9) by 35.39 Ma (81.04 mcd). Non-radiogenic values continue to decrease from 29.98 Ma (72.56 mcd) to the top of the record, ultimately approaching an ε_{Nd} signal <-13.

Samples from Site 1263 are 52.99 to 7.69 Ma in age (276.3 to 18.09 mcd). The base of the record (**Figure 9**) has $\varepsilon_{Nd}(t)$ values of >-10 to >-9, with one notable outlier of ~-6.7 at 50.07 Ma (238.51 mcd). From 39.37 to 31.44 Ma (138.12 to 63.08 mcd), $\varepsilon_{Nd}(t)$ values increase, peaking at just greater than -8.5. Although there is a gap in data, values decrease from ~-10 at ~32 Ma to a minimum of -11.4 at 7.69 Ma.

The record from Site 1264 (**Fig. 9**) begins later than the other two, extending from 26.96 to 5.20 Ma (273.12 to 61.88 mcd). Values are ~-10 at the bottom of the record, but at 15.53 Ma (187.39 mcd), the data trend towards a more non-radiogenic signal. The minimum value of -11.4 occurs at 5.20 Ma.

When all sites are plotted together (**Figure 10**), the data indicate a first-order linear trend of an initial transition from relatively non-radiogenic values (~-10) at ~55 Ma to more radiogenic values (about -8.5) at ~32 Ma. From ~32 Ma to 3.85 Ma, the Nd signal becomes more non-radiogenic, approximately -12.3 at the top of the record.

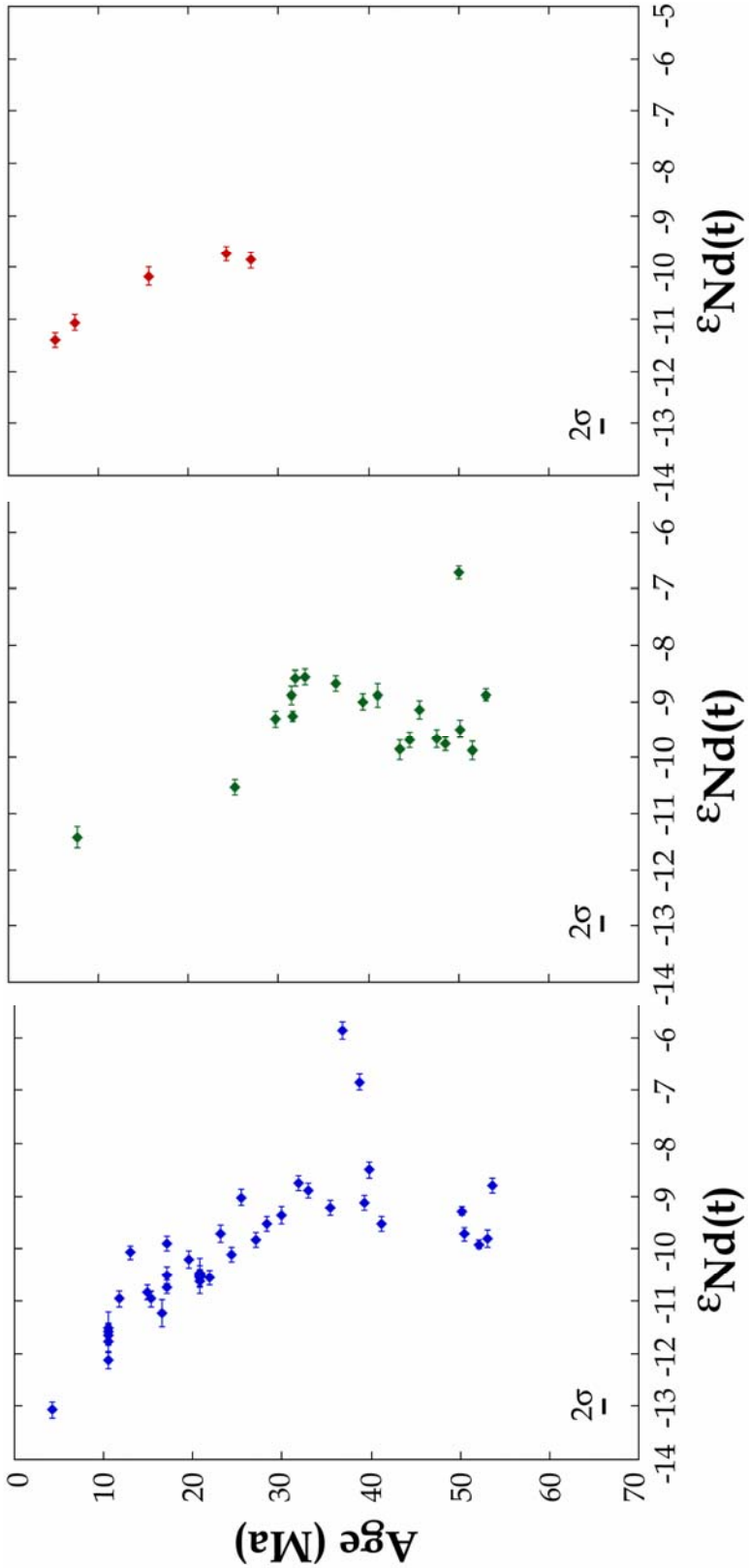

Figure 9. Epsilon-Nd records generated in this study from Sites 1262, 1263, and 1264.

Table 2. ε_{Nd} results

	Core	Sect	top	base	depth mbsf	depth mcd	age Ma	143/144	%SE	abs err	$\varepsilon_{Nd}(0)$	error	I_tCHUR	$(143/144)_t$	$\varepsilon_{Nd}(t)$
Site 1262	3H	3	117	119	23.17	30.48	4.30	0.5120096	0.0008	8E-06	-12.26	0.16	0.5126325	0.5119625	-13.07
Hole A	5H	1	117	119	39.17	48.13	10.57	0.5120501	0.0008	8E-06	-11.47	0.16	0.5126244	0.5120030	-12.12
	5H	2	117	119	40.67	49.63	11.76	0.5121081	0.0008	8E-06	-10.34	0.16	0.5126229	0.5120610	-10.96
	5H	3	117	119	42.17	51.13	12.95	0.5121524	0.0006	6E-06	-9.47	0.12	0.5126213	0.5121053	-10.07
	5H	4	117	119	43.67	53.63	14.94	0.5121104	0.0007	7E-06	-10.29	0.14	0.5126188	0.5120633	-10.84
	5H	5	117	119	45.17	54.13	15.34	0.5121035	0.0008	8E-06	-10.43	0.16	0.5126183	0.5120564	-10.96
	5H	6	117	119	46.67	55.63	16.53	0.5120879	0.0013	1E-05	-10.73	0.26	0.5126167	0.5120408	-11.24
	5H	7	37	39	47.37	56.33	17.08	0.5121250	0.0008	8E-06	-10.01	0.16	0.5126160	0.5120779	-10.50
	5H	CC	15	17	47.72	56.34	17.09	0.5121557	0.0007	7E-06	-9.41	0.14	0.5126160	0.5121086	-9.90
	6H	1	117	119	48.67	59.42	19.54	0.5121371	0.0008	8E-06	-9.77	0.16	0.5126129	0.5120900	-10.20
	6H	2	117	119	50.17	60.92	20.73	0.5121171	0.0009	9E-06	-10.16	0.18	0.5126113	0.5120700	-10.56
	6H	3	117	119	51.67	62.42	21.92	0.5121163	0.0007	7E-06	-10.18	0.14	0.5126098	0.5120692	-10.55
	6H	4	117	119	53.17	63.92	23.12	0.5121575	0.0008	8E-06	-9.37	0.16	0.5126083	0.5121104	-9.71
	6H	5	117	119	54.67	65.42	24.31	0.5121361	0.0007	7E-06	-9.79	0.14	0.5126067	0.5120890	-10.10
	6H	6	117	119	56.17	66.92	25.50	0.5121902	0.0008	8E-06	-8.74	0.16	0.5126052	0.5121431	-9.02
	7H	1	50	52	57.50	68.89	27.07	0.5121468	0.0007	7E-06	-9.58	0.14	0.5126032	0.5120997	-9.82
	7H	2	50	52	59.00	70.39	28.26	0.5121604	0.0007	7E-06	-9.32	0.14	0.5126016	0.5121133	-9.53
	7H	3	117	119	57.50	68.89	27.07	0.5121468	0.0007	7E-06	-9.58	0.14	0.5126032	0.5120997	-9.82
	7H	5	50	52	59.00	70.39	28.26	0.5121604	0.0007	7E-06	-9.32	0.14	0.5126016	0.5121133	-9.53
	7H	6	50	52	61.17	72.56	29.98	0.5121668	0.0008	8E-06	-9.19	0.16	0.5125994	0.5121197	-9.36
	7H	5	50	52	63.50	74.89	31.84	0.5121964	0.0007	7E-06	-8.61	0.14	0.5125970	0.5121493	-8.74
	7H	6	50	52	65.00	76.39	32.95	0.5121868	0.0007	7E-06	-8.80	0.14	0.5125956	0.5121397	-8.89
	8H	1	50	52	67.00	81.04	35.39	0.5121671	0.0007	7E-06	-9.19	0.14	0.5125925	0.5121200	-9.22
	8H	2	50	52	68.42	82.46	36.75	0.5123370	0.0008	8E-06	-5.87	0.16	0.5125907	0.5122899	-5.87
	8H	3	117	119	70.49	84.53	38.72	0.5122846	0.0008	8E-06	-6.89	0.16	0.5125882	0.5122375	-6.84
	8H	4	50	52	71.02	85.06	39.22	0.5121668	0.0007	7E-06	-9.19	0.14	0.5125875	0.5121197	-9.13
	8H	5	50	52	71.63	85.67	39.81	0.5121984	0.0008	8E-06	-8.58	0.16	0.5125868	0.5121513	-8.50
	8H	6	50	52	73.06	87.10	41.17	0.5121441	0.0007	7E-06	-9.63	0.14	0.5125850	0.5120970	-9.52
	9H	1	50	52	76.50	91.71	50.24	0.5121447	0.0004	4E-06	-9.62	0.08	0.5125734	0.5120976	-9.28
	9H	2	50	52	78.00	93.21	50.44	0.5121220	0.0006	6E-06	-10.07	0.12	0.5125731	0.5120749	-9.72
	10H	3	117	119	89.67	105.78	52.12	0.5121102	0.0004	4E-06	-10.30	0.08	0.5125709	0.5120631	-9.91

Table 2. continued

	Core	Sect	top	base	depth mbsf	depth mcd	age Ma	143/144	%SE	abs err	$\varepsilon_{Nd}(0)$	err	I_tCHUR	$(143/144)_t$	$\varepsilon_{Nd}(t)$
	11H	3	117	119	99.17	115.22	53.12	0.5121142	0.0008	8E-06	-10.22	0.16	0.5125696	0.5120671	-9.81
	12H	3	117	119	108.67	125.28	53.65	0.5121654	0.0007	7E-06	-9.22	0.14	0.5125690	0.5121183	-8.79
Site 1263	3H	3	117	119	15.97	18.09	7.69	0.5120899	0.0009	9E-06	-10.69	0.18	0.5126281	0.5120428	-11.42
Hole A	4H	3	117	119	25.47	29.30	25.22	0.5121135	0.0007	7E-06	-10.23	0.14	0.5126056	0.5120664	-10.52
	6H	3	117	119	44.47	51.72	29.68	0.5121693	0.0007	7E-06	-9.14	0.14	0.5125998	0.5121222	-9.32
	7H	3	117	119	53.97	63.08	31.44	0.5121892	0.0008	8E-06	-8.75	0.16	0.5125975	0.5121421	-8.89
	8H	3	117	119	63.47	74.18	31.65	0.5121699	0.0005	5E-06	-9.13	0.10	0.5125973	0.5121228	-9.26
	9H	3	117	119	72.97	84.74	31.85	0.5122044	0.0007	7E-06	-8.46	0.14	0.5125970	0.5121573	-8.58
	10H	3	117	119	82.47	94.26	32.95	0.5122045	0.0007	7E-06	-8.46	0.14	0.5125956	0.5121574	-8.55
	12H	3	77	79	101.07	114.80	36.38	0.5121941	0.0007	7E-06	-8.66	0.14	0.5125912	0.5121470	-8.67
	14H	3	107	109	120.37	138.12	39.37	0.5121731	0.0007	7E-06	-9.07	0.14	0.5125874	0.5121260	-9.00
	15H	3	117	119	129.97	150.49	41.06	0.5121764	0.0011	1E-05	-9.00	0.22	0.5125852	0.5121293	-8.89
	16H	3	117	119	139.47	161.36	43.54	0.5121235	0.0009	9E-06	-10.04	0.18	0.5125820	0.5120764	-9.86
	17H	3	117	119	148.97	171.99	44.55	0.5121309	0.0007	7E-06	-9.89	0.14	0.5125807	0.5120838	-9.69
	18H	3	117	119	158.47	182.41	45.62	0.5121576	0.0008	8E-06	-9.37	0.16	0.5125793	0.5121105	-9.15
	20H	3	117	119	177.47	205.24	47.63	0.5121282	0.0008	8E-06	-9.94	0.16	0.5125767	0.5120811	-9.67
	22H	3	117	119	196.21	228.55	48.55	0.5121228	0.0006	6E-06	-10.05	0.12	0.5125755	0.5120757	-9.75
	23H	3	117	119	205.96	238.51	50.07	0.5122767	0.0006	6E-06	-7.05	0.12	0.5125736	0.5122296	-6.71
	24H	3	117	119	212.27	246.92	50.12	0.5121340	0.0008	8E-06	-9.83	0.16	0.5125735	0.5120869	-9.49
	26H	3	117	119	226.77	263.62	51.61	0.5121128	0.0008	8E-06	-10.25	0.16	0.5125716	0.5120657	-9.87
	27H	3	117	119	236.27	276.30	52.99	0.5121620	0.0005	5E-06	-9.29	0.10	0.5125698	0.5121149	-8.88
Site 1264	6H	3	117	119	51.47	61.88	5.20	0.5120941	0.0007	7E-06	-10.61	0.14	0.5126313	0.5120470	-11.40
Hole A	10H	3	117	119	89.47	105.78	7.38	0.5121087	0.0008	8E-06	-10.325	0.1598	0.5126285	0.5121024	-11.06
	18H	3	117	119	165.47	187.39	15.53	0.5121439	0.0009	9E-06	-9.6384	0.1798	0.5126180	0.5121306	-10.17
	25H	2	117	119	230.47	261.25	24.21	0.5121549	0.0007	7E-06	-9.4238	0.1399	0.5126068	0.5121342	-9.74
	26H	3	117	119	241.47	273.12	26.96	0.5121450	0.0008	8E-06	-9.6169	0.1598	0.5126033	0.5121219	-9.86

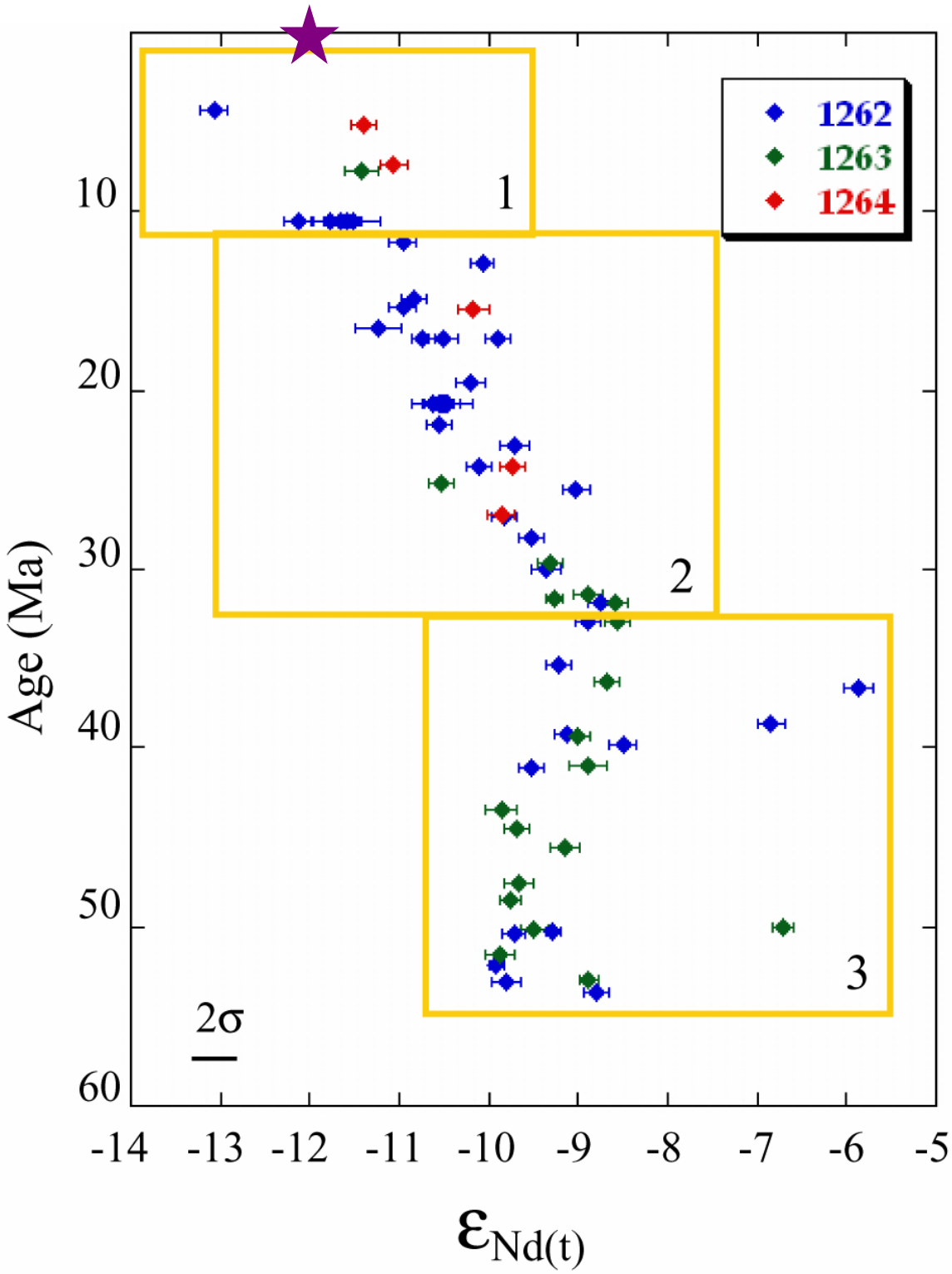

Figure 10. Results of Sites 1262, 1263 and 1264, showing three distinct temporal intervals. Star represents modern-day bottom-water $\varepsilon_{Nd}(t)$ at Walvis Ridge.

5. DISCUSSION

Our data spans the past ~53 Ma, through the transition from the last major "greenhouse" climate of the Cenozoic into the present "icehouse" conditions. One noteworthy feature of the dataset is that all three sites record similar values for most of the time interval represented (**Figure 10**). In addition, the three records demonstrate coherent temporal trends, within the limits of the age model. The coherence of values and trends indicates that the same water mass influenced all three sites throughout the record.

Interpretations of the Nd isotope data begin with the assumption that the Southern Ocean was the dominant deep-water formation region for most of the Cenozoic. Although there is still a dearth of measurements to support this claim, there are several lines of indirect evidence to suggest it.

First, it is unlikely that the North Atlantic was a deep-water source region in the Early Cenozoic. At this time, the Greenland and Norwegian Seas had just begun to open and were still incipient basins. Planktonic $\delta^{18}O$ records from the Bay of Biscay estimate SSTs in the early northern North Atlantic were as high as ~23° C [*Charisi and Schmitz*, 1996]. These small basins with warm buoyant surface waters would have been unlikely to produce any significant volume of deep water. Additionally, benthic $\delta^{13}C$ records indicate that deep waters in the western North Atlantic were nutrient-enriched in the early Eocene (57-52 Ma) and hence "old" and unlikely to have formed nearby [*Katz and Miller*, 1991].

Second, it is unlikely that our record indicates the North Pacific influence on deep waters. This region is rimmed by active areas of arc volcanism, the drainage of which yields waters of a more radiogenic ε_{Nd} signal. Pacific Fe-Mn crusts record intermediate- and deep-water ε_{Nd} values between -5.22 and -4.07 from ~57 to 47 Ma [*Ling et al.*, 1997]. Although *Thomas* [2004] demonstrated the evidence of some North Pacific deep-water production at Shatsky Rise from ~65-45 Ma, our ε_{Nd} record over this

interval points to a deep-water source far too non-radiogenic (~-9.2 to -10.3; 1 on **Figure 10**) to have been fully formed in the North Pacific.

Third, modeling studies [*Brady et al*., 1998; *DeConto et al*., 2000] suggest a Southern Ocean deep-water source for the Late Cretaceous, and likely suggest similar conditions for the Early Cenozoic as well. Late Cretaceous (~70 Ma) global bottom water temperatures were possibly as high as ~15°C [*Savin,* 1977; *Saltzman and Barron,* 1982], compared to ~12°C at time of peak warmth in the early Paleogene (~50 Ma). Paleogeography used in the model is similar to ~50 Ma conditions, including an open Tethys and closed Tasman Gateway, Drake Passage, and northern North Atlantic basins, but a more restricted southern Atlantic and Southern Ocean. For latitudes between 60-90°, these models predict sea-surface temperatures 10-12° C warmer than the present. Areas of deep convection (from 3300-5000 m water depth) are predicted at Southern Hemisphere high latitudes. Downwelling of warm saline waters originating in the Southern Atlantic would give rise to the small meridonal thermal gradients of the Late Cretaceous and Early Cenozoic. In this scenario, the mechanism of downward convection is similar to that seen presently in the North Atlantic, where density increases through cooling of already salty waters. The dataset is characterized by three distinct temporal trends (from ~53 to ~34 Ma, ~34 to ~10 Ma, and ~10 Ma to ~3 Ma), and we discuss each separately in the following sections.

5.1~53 to ~34 Ma

We have assumed that relatively non-radiogenic values at the base of the record (1 on **Figure 10**) reflect a Southern Ocean deep water source. Over the next ~20 Ma, ε_{Nd} values shift towards more radiogenic values, from ~-10 to ~-8.5. We interpret this shift to imply a change in Nd delivery to the Southern Ocean, as opposed to a change in deep-water formation region. Climatic and tectonic changes in the North Atlantic over this interval likely were not considerable enough for the region to begin volumetrically significant deep-water production. In addition, Pacific deep-water ε_{Nd} values were too

high (~4.5 to -4, *Ling et al.* [1997]) compared to those seen at Walvis Ridge (~-8, peaking at ~-6) for the Pacific to have been the dominant source region. Thus, the Southern Ocean still would have been the most likely site where deep-water formation occurred.

There are several explanations for the long-term radiogenic shift. The first possibility is that the ε_{Nd} composition of the Southern Ocean became more radiogenic due to an increased surface contribution from the Pacific. While the Drake Passage was still blocking deep flow at 40 Ma [*Lawver and Gahagen,* 2003], it is possible that a wind-driven circulation may have brought Pacific surface waters eastwards through a relatively shallow sill. It is also possible that Pacific surface waters may have been able to enter the Atlantic sector of the Southern Ocean through the trans-Antarctic seaway. *Lawver and Gahagan* [2003] show this conduit as at least partially open to flow from 50-33 Ma (**Figure 11**).

Radiogenic Nd also may have entered Southern Ocean surface waters through increased arc-volcanism in the Scotia Sea as the Drake Passage opened. *Eagles and Livermore* [2002] constrain rifting off the tip of the Antarctic Peninsula in the Powell Basin to ~40-29.7 Ma. Additionally, *Barber et al*. [1991] establish that rift-associated volcanism was extensive in the basin throughout the interval. Evidence of this volcanic activity is possibly found at Walvis Ridge. Both Sites 1262 and 1263 have prominent ash layers at ~39-40 Ma (85.25 mcd and 155.7 mcd, respectively).

In addition to the Drake Passage, other deep-water gateways were opening during this interval. Initial deepening of the Tasman Gateway began prior to ~35.5 Ma and further deepening in the region occurred from ~35.5 to 33.5 Ma [*Exon, Kennett, Malone, et al,* 2001]. Warm surface waters from the proto-East Australian Current were now able to exchange with cooler surface waters originating in the Pacific. Combined with initial opening in the Drake Passage, a shallow precursor to the ACC was emerging.

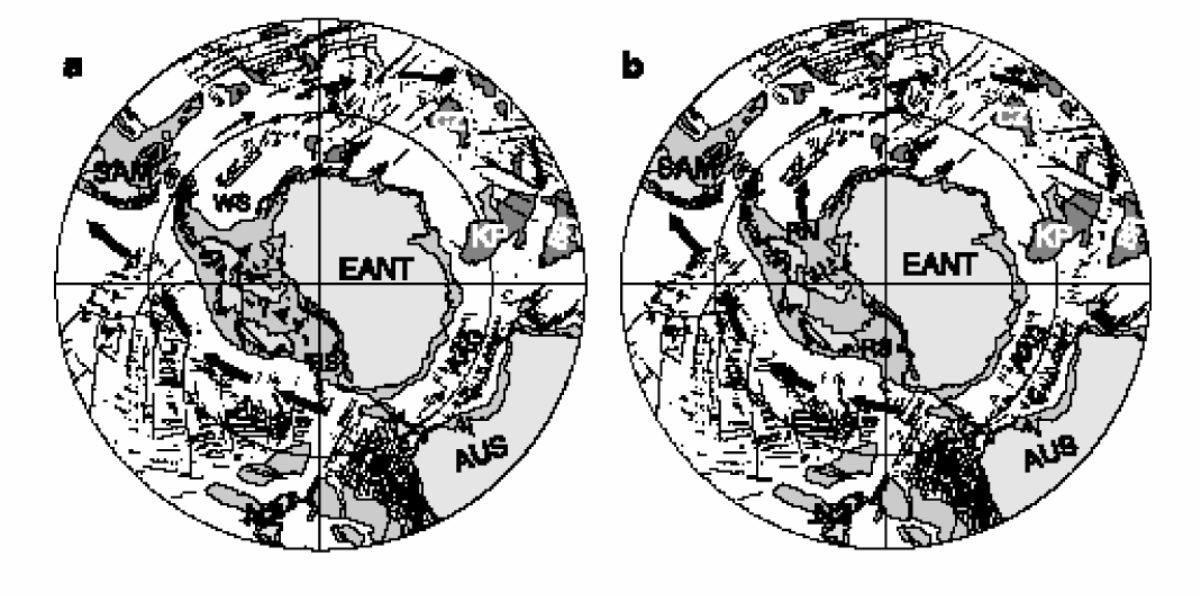

Figure 11. 34 Ma (**a**, *left*) and 33 Ma (**b**, *right*) polar reconstructions. From *Lawver and Gahagan* [2003].

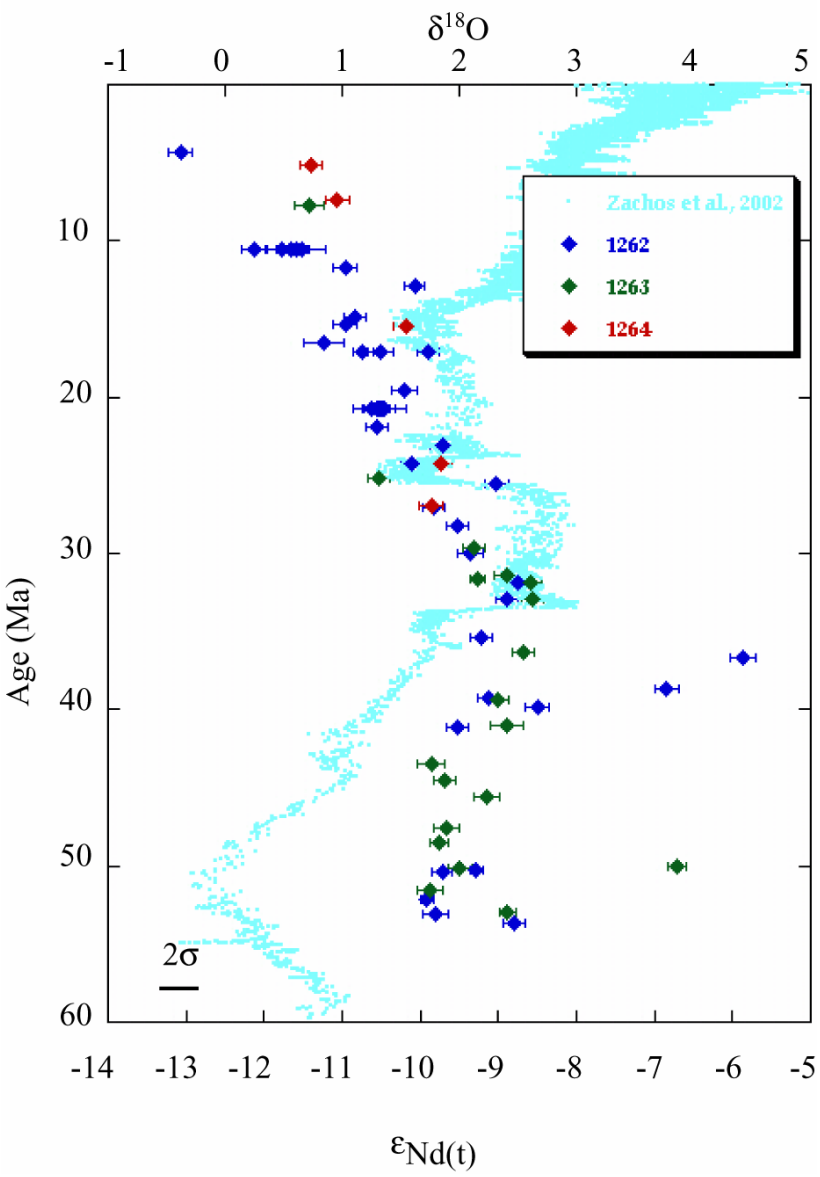

Figure 12. Oxygen stable isotope data with major climatic events from *Zachos et al.* [2001] plotted with ε_{Nd} record generated in this study.

Concurrent with the development of surface layer of proto-ACC, deep waters were cooling. The ~50-34 Ma interval displays a global increase in benthic foraminiferal $\delta^{18}O$ values (**Figure 12**). Average bottom water temperatures at ~34 Ma had decreased to ~4.5°C, down from a maximum of ~12°C at ~50 Ma [*Zachos et al.,* 2001]. As these deep waters likely had formed in the southern polar region, Southern Ocean surface waters must also have cooled to ~4.5°C. This cooling marks the end of the "greenhouse" regime and the beginning of the "icehouse" climate.

Although climatic and tectonic boundary conditions were evolving over this era, deep waters were still most likely forming at southern high latitudes. Instead of a change in the region of downwelling, we contend that some combination of the above factors likely drove changes in the delivery of more radiogenic waters to the Southern Ocean. Although these changes may have driven the radiogenic shift in Nd isotope values, competing processes must be invoked to explain the subsequent trend toward more non-radiogenic values.

5.2 ~34 to ~10 Ma

Comparison of the ε_{Nd} record with oxygen isotope records provides a climatic context for interpreting trends in terms of changes in weathering rates and patterns. The peak in radiogenic values at ~32 Ma is approximately coincident with the Oi-1 glaciation on the Antarctic continent (**Figure 12**). The Oi-1 glaciation is believed to mark the onset of ice accumulation on Antarctica and commonly represents the transition between the "greenhouse" and the initial "icehouse" [*Zachos et al.,* 2001]. Oxygen isotope values drop sharply at ~33 Ma, implying bottom water temperatures ~0°C and permanent Antarctic ice [*Zachos et al.,* 2001]. A recent modeling study [*DeConto and Pollard,* 2003] suggests that a decrease in atmospheric CO_2 coupled with orbital parameters and ice-climate feedbacks may have triggered the onset of Antarctic glaciation at ~34 Ma.

From ~30-15 Ma, Nd isotope values become more non-radiogenic (2 on **Figure 10**), coinciding with an overall decrease of benthic foraminiferal $\delta^{18}O$ values (**Figure 12**). By ~31-30 Ma, both the Drake Passage and Tasman Gateway were likely fully open [*Exon, Kennett, Malone, et al.,* 2001; *Lawver and Gahagan,* 2003; *Stickley et al,* 2004], allowing for continuous deep and surface exchange between the Atlantic and Pacific Oceans. The creation of one cold pole could conceivably intensify the Polar Front, and further change the weathering regime around the Southern Ocean. Although the Greenland, Norwegian and Labrador Seas matured through this interval, our record does not yet reflect the influence of a North Atlantic-sourced deep water at Walvis Ridge. It is more likely that the build-up of Antarctic continental ice and concurrent global cooling through the Oligocene and early Miocene increased the weathering of more non-radiogenic cratonic rocks from Antarctica into the Southern Ocean.

A study of the East Kerguelen sediment drift (ODP Site 745; *Joseph et al*. [2002]), shows that during times of continental ice sheet advance the rate of erosion increases, in turn increasing the amount of Antarctic-derived sediments being delivered to the deep sea. In addition to the increase physical weathering, the onset of permanent ice cover may also shift the locus of weathering on the Antarctic continent. The lithology of Antarctica varies regionally: basement rocks range in age from Mid-Cretaceous (106 Ma; *Riley et al*. [2003]) to Mesoproterozoic (1.2 Ga; *Andronikov et al*. [1998]) and have been derived from partial melts of both the lithosphere and asthenosphere [*Riley et al*., 2003]. Mantle plume hot spots have also been identified on the Antarctic continent (**Figure 13**). Preferential weathering of any one of the above rock types would deliver a different ε_{Nd} signal to the Southern Ocean. As weathering patterns changed on the Antarctic continent, so too would the dissolved $^{143}Nd/^{144}Nd$ ratio delivered to the adjacent water masses.

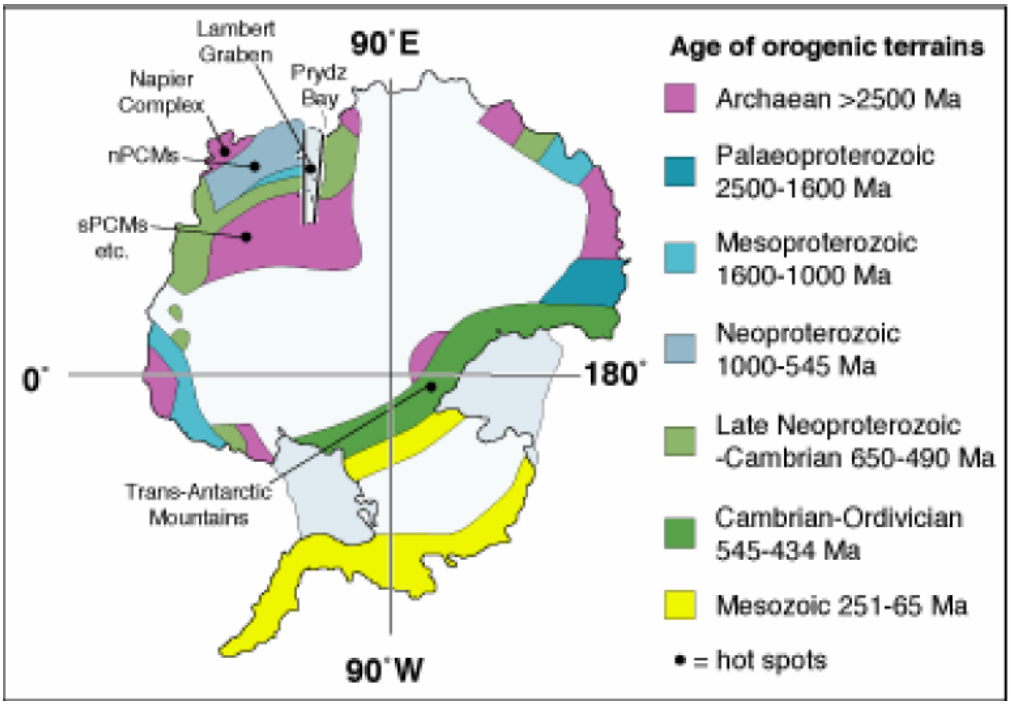

Figure 13. Geologic Map of Antarctica. *http://web.earthsci.unimelb.edu.au/antarctica/tecProvinces.html*

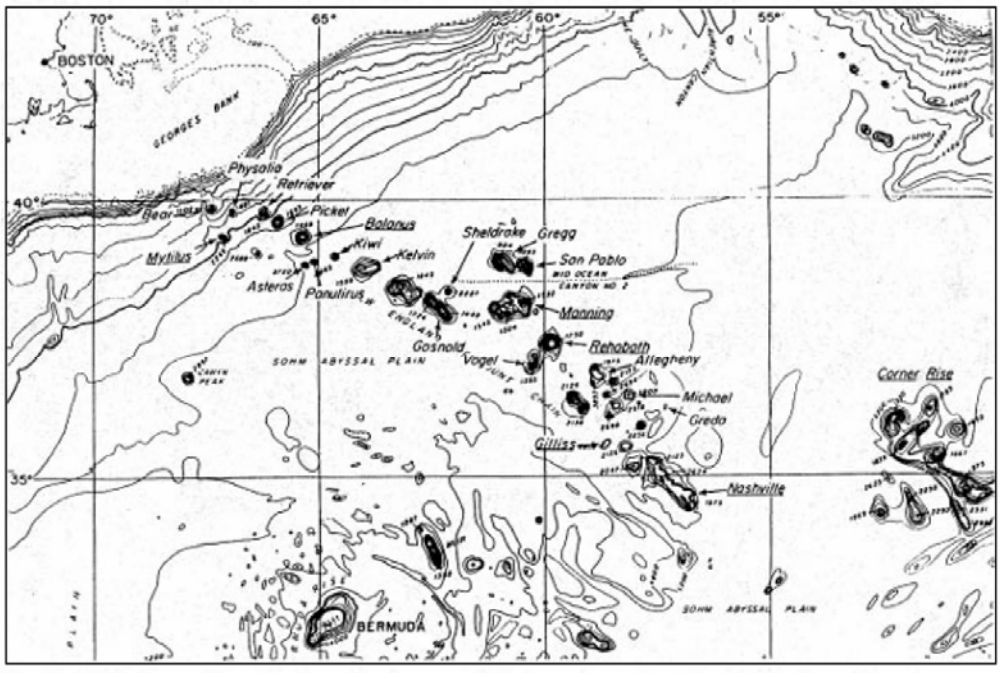

Figure 14. Location of San Pablo Seamount in western North Atlantic. From *Houghton et al.* [1977].

5.3 ~10 to ~3 Ma

The Site 1262 record potentially shows the evolution of proto-North Atlantic Deep Water (NADW) in the latest part of the record, beginning at ~10 Ma. The shift from ~-10 at 10-18 Ma to <-12 ε_{Nd} at 3 Ma (3 on **Figure 10**) likely represents the initial advection of North Atlantic deep waters to Walvis Ridge. Values of <-12 are consistent with present day NADW in the southeastern Atlantic (**Figure 4**). It is possible that some influence from the North Atlantic began as early as ~18 Ma, when ε_{Nd} values first drop below -11.

Although the data are sparse, trends recorded at the three sites suggest that the deepest site recorded the proto-NADW signal earlier than the shallower two. We had assumed that, in its initial stages, NADW was a relatively slim mass that grew vertically downward as convection grew more vigorous and the flux increased. The results in this interval were therefore unexpected, for they suggest the "bottom-up" growth of NADW as opposed to "top-down". In any case, formation of intermediate, deep, and bottom waters at both poles had begun by at least 10 Ma (though possibly earlier), and indicates the initiation of a modern-type of water mass structure throughout the Atlantic basin.

5.4 Atlantic deep-water evolution

Prior to this study, the only long-term Cenozoic record of Atlantic Nd composition was from a Fe-Mn crust [*Burton et al.,* 1997], which was dredged from San Pablo seamount, located southeast of Georges Bank in the western North Atlantic (**Figure 14**). It is interesting to compare the two records (**Figure 15**). There is less variation in the crust record >~10 Ma, and there is a slight offset from the fish debris record between ~10-0 Ma. The San Pablo record shows less detail than the Walvis Ridge record. Additionally, age models are uncertain for crusts older than 10 Ma, as constraints are based on $^{10}Be/^{9}Be$ dates that are linearly extrapolated for ages older than the effective 10 million year lifetime of ^{10}Be ($t_{½}$ = 1.5 my). Hence this record is less

suitable for understanding specific trends in the temporal and vertical evolution of Atlantic water-mass composition.

At the base of both records, ε_{Nd} values are between ~-10.5 and -9 until ~42 Ma. Diffusion of waters draining older Canadian rocks may cause this record to be slightly less radiogenic than the Walvis Ridge or Maud Rise (to be discussed below) records. As the Walvis values trend towards a more radiogenic source in the late Eocene/early Oligocene (~38-32 Ma), the Fe-Mn crust values do not. The San Pablo seamount currently lies beneath the Deep Western Boundary Current, on the western side of the Mid-Atlantic Ridge. The crust was retrieved from a depth of 1850m, shallower than any of the Walvis Ridge sites. It is possible that the crust is recording the signal of a shallower water mass distinct from the deeper waters bathing Walvis Ridge and Maud Rise. The crust record confirms the influence of North Atlantic-sourced deep waters by as late as ~10 Ma, though given the gap in data from ~10-18 Ma, this record cannot provide any evidence of an earlier North Atlantic influence.

Comparison of the Walvis Ridge records in the southeastern Atlantic to data from Maud Rise [*Scher and Martin,* 2004] in the Southern Ocean reveal regional trends in deep-water composition through the Paleogene (**Figure 16**). ODP Site 689 (64.31°S, 3.06°E) is located in the Atlantic sector of the Southern Ocean at a present-day depth of 2080 m. Both records show coherent trends: an increase in values peaking ~35-33 Ma, then a decrease in values until ~18 Ma. The two records begin to diverge during the shift at ~32 Ma, with the Walvis Ridge values becoming more non-radiogenic than the Maud rise values and remain this way until ~18 Ma, where the Site 689 record stops.

Because both records show a coeval radiogenic trend and peak implies that they were influenced by the same water mass, the composition of which changed regionally. The divergence of the two records from ~32-18 Ma is also significant. A possible scenario causing this divergence is tied to overall Southern Hemisphere cooling. Prior to the onset of Southern Hemisphere glaciation, there may have been little stratification in the water column. The intensification of Antarctic Circumpolar Current jets may have

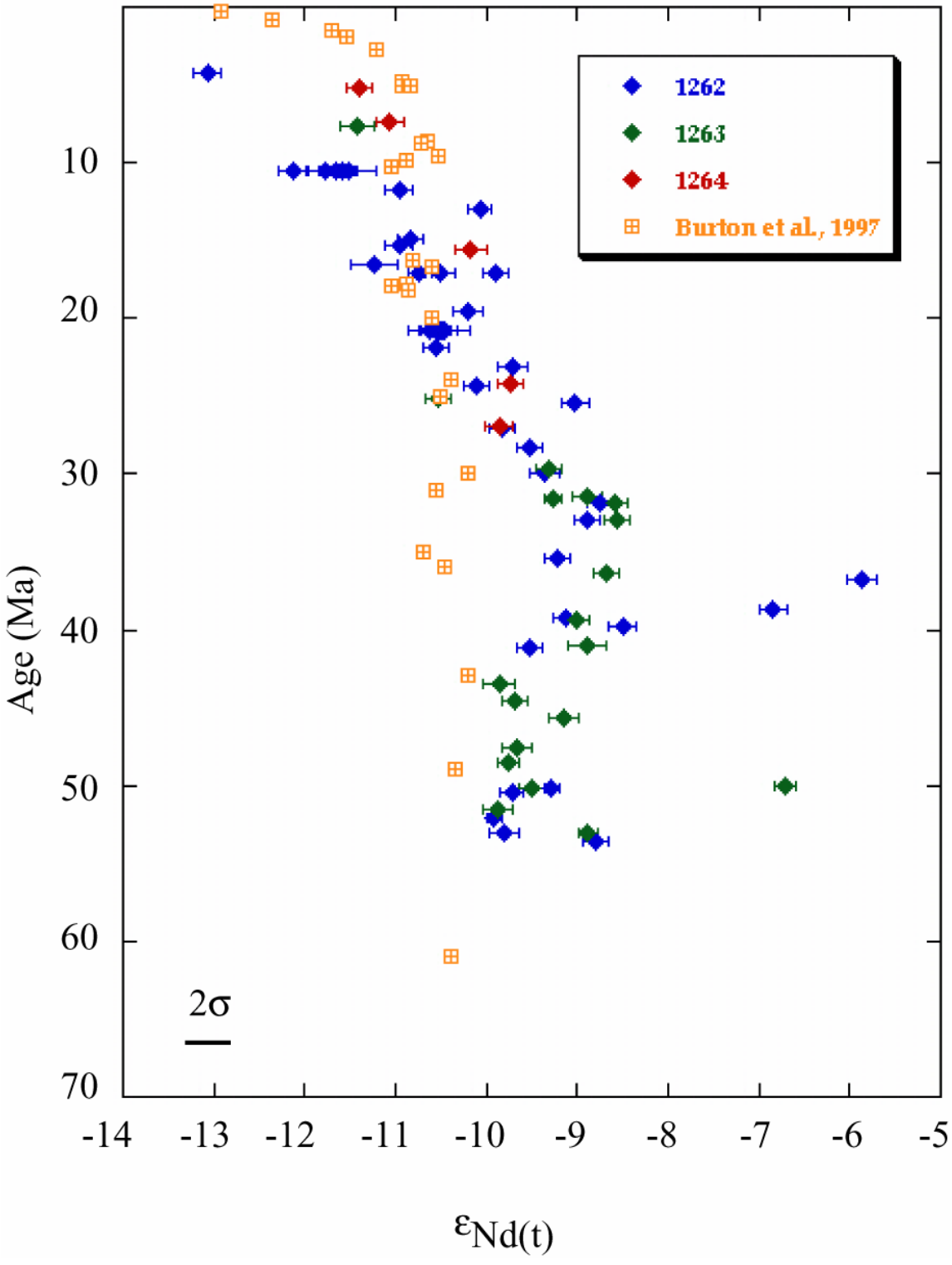

Figure 15. Comparison of San Pablo Seamount ε_{Nd} record from *Burton et al.* [1997] with the Walvis Ridge record.

led to the formation of both deep and intermediate waters. Currently, Antarctic Intermediate Water (AAIW) is a relatively fresh water mass that forms by subsidence of super-cooled waters to intermediate depths. Although both AAIW and AABW form in the Antarctic, present-day AAIW forms in the Antarctic Polar Frontal Zone, whereas AABW forms in the continental shelf region of Antarctica. Deep waters forming in this region would show a less radiogenic signal, due to the delivery of dissolved Nd from the weathering and drainage of continental rocks. Intermediate waters from the Antarctic Polar Frontal Zone receive more radiogenic Nd from the subduction of Pacific surface waters. *Jeandel* [1993] (**Figure 4,** *inset*) showed that contemporary ε_{Nd} values for AAIW are ~-8 to -6, more radiogenic than the underlying NADW or AABW. Similarly, the Maud Rise data set indicates that intermediate waters were also more radiogenic than deep and bottom waters from ~32 to at least 18 Ma. We believe that the difference in deep-water versus intermediate-water ε_{Nd} over this interval indicates that deep-water production was now distinct from intermediate-water production.

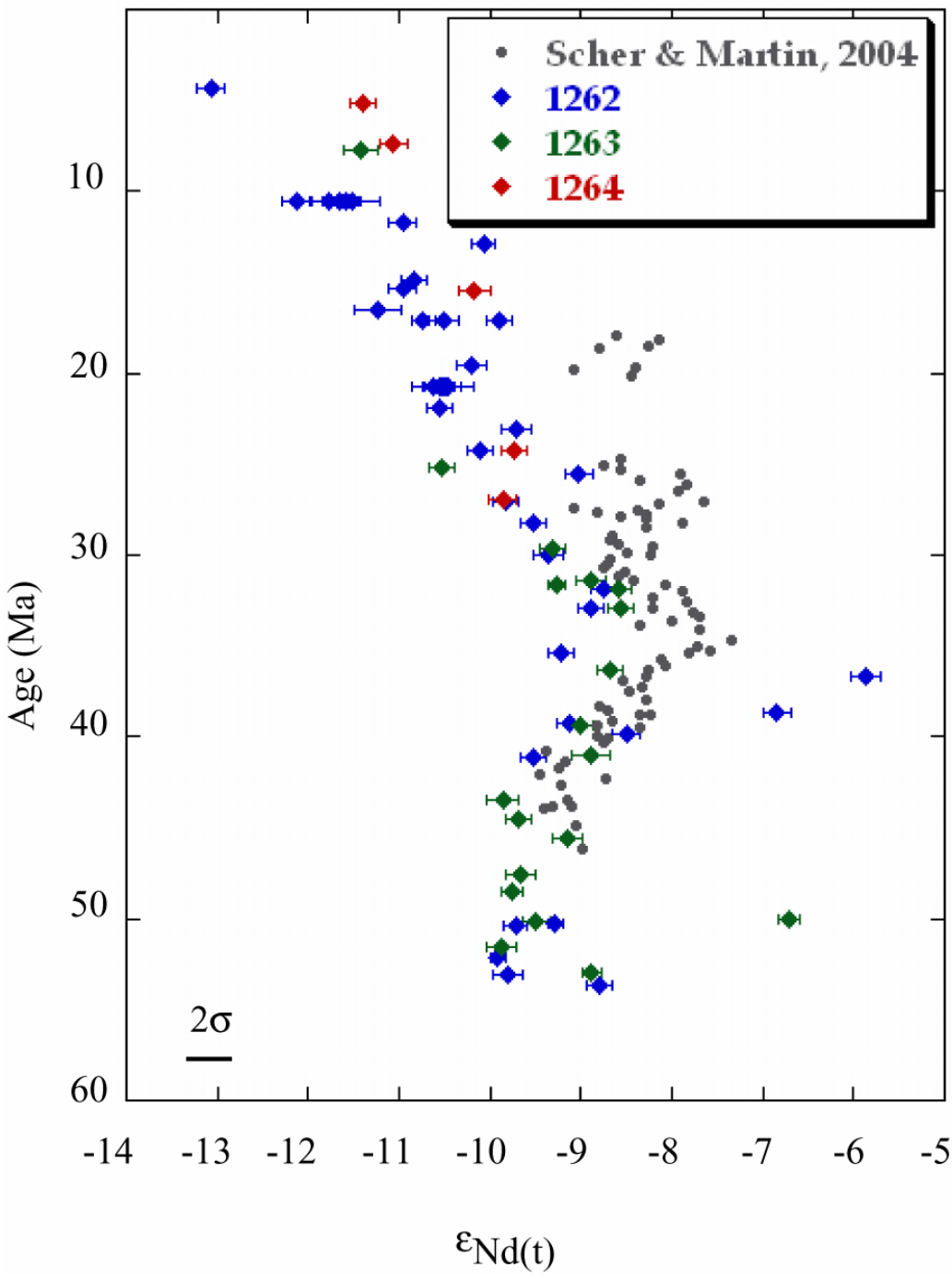

Figure 16. Walvis Ridge [*this study*] and Maud Rise [*Scher and Martin*, 2004] ε_{Nd} records. Note divergence of trends at ~32 Ma.

6. CONCLUSIONS

1. The data likely reflect dominance of a Southern Ocean deep-water source throughout most of the Cenozoic, with the initial indication of deep waters from the North Atlantic possibly beginning as early as ~18 Ma.
2. An increased contribution of Pacific waters to regions of convection in the Southern Ocean due to tectonic gateway changes is likely responsible for the radiogenic shift seen from ~53-34 Ma.
3. Onset and rapid growth of Southern Hemisphere glaciation at ~34 Ma is the most probable mechanism for the trend back to non-radiogenic values from ~34-10 Ma.
4. The influence of a North Atlantic-sourced deep water is evident by ~10 Ma. The deepest site shows this influence first followed by the shallower two, reflecting the growth of proto-NADW and evolution of water mass stratification.
5. Comparison of our record with an Atlantic Fe-Mn crust record shows more detail, specifically the radiogenic trend, inflection point, and recovery of non-radiogenic values. However, both records begin to trend towards modern values around ~10 Ma.
6. Regional data from Maud Rise shows coherent trend with Walvis Ridge from ~48-32 Ma. The divergence of the two records from ~32-18 Ma may imply the onset of intermediate-water production distinct from deep-water production.

REFERENCES

Abouchami, W., S.J. G. Galer and A. Koschinsky (1999), Pb and Nd isotopes in NE Atlantic Fe-Mn crusts: Proxies for trace metal paleosources and paleocean circulation, *Geochim. Cosmochim. Acta, 63*, 1489-1505.

Andronikov, A.V., S.F. Foley and B.V. Beliatsky (1998) Sm-Nd and Rb-Sr isotope systematics of the East Antarctic Manning Massif alkaline trachybasalts and the development of the mantle beneath the Lambert-Amery rift, *Mineral. Petrol., 63,* 243-261.

Barber, P.L., P.F. Barker and R.J. Pankhurst (1991) Dredged rocks from Powell Basin and the South Orkney Microcontinent, in: *Geological Evolution of Antarctica,* edited by M.R.A. Thomson et al., pp. 361-367, Cambridge University Press, Cambridge.

Boyle, E.A. (1981), Cadmium, zinc, copper, and barium in foraminiferal tests. *Earth Planet. Sci. Lett., 53*, 11-35.

Boyle, E.A. and L.D. Keigwin. (1985), Comparison of Atlantic and Pacific paleochemical records for the last 250,000 years: Changes in deep-ocean circulation and chemical inventories. *Earth Planet. Sci. Lett., 76*, 135-150.

Brady, E.C., R.M. DeConto and S.L. Thompson (1998), Deep water formation and poleward ocean heat transport in the warm climate extreme of the Cretaceous (80 Ma), *Geophys. Res. Lett., 25,* 4205-4208.

Brass, G.W., J.R. Southam and W.W. Peterson (1982), Warm saline bottom water in the deep ocean. *Nature, 296,* 620-623.

Broecker, W.S., R. Gerard, M. Ewing and B.C. Heezen (1960), Natural radiocarbon in the Atlantic Ocean, *J. Geophys. Res., 65*, 2903-2931.

Burton, K.W., H.-F. Ling and R.K O'Nions (1997), Closure of the Central American Isthmus and its effect on North Atlantic Deep Water formation, *Nature 386*, 382-385.

Burton, K.W., D.-C. Lee, J.N. Christensen, A.N. Halliday and J.R. Hein (1999) Actual timing of neodymium isotopic variations recorded by Fe-Mn crusts in the western North Atlantic, *Earth Planet. Sci. Lett., 171,* 149-156.

Cande, S.C. and D.V. Kent (1995), Revised calibration of the geomagnetic polarity timescale for the Late Cretaceous and Cenozoic. *J. Geophys. Res., 100*, 6093-6095.

Charisi, S.D. and B. Schmitz (1996), Early Eocene palaeoceanography and palaeoclimatology of the eastern North Atlantic: stable isotope results for DSDP Hole

550, in *Correlation of the Early Paleogene in Northwest Europe,* Geological Society Special Publication No. 101, edited by R.W. Knox et al., pp. 457-472, Geological Society of London, London.

Colling, A. (2001), *Ocean Circulation,* The Open University and Butterworth-Heinemann, Milton-Keynes, 213-223.

Crowley. T.J. (1998), Significance of tectonic boundary conditions for paleoclimate simulations, in *Tectonic Boundary Conditions for Climate Reconstructions*, Oxford Monographs on Geology and Geophysics No. 39, edited by T.J. Crowley and K.C. Burke, pp. 3-17, Oxford University Press, Oxford.

DeConto, R.M., E.C. Brady, J. Bergengren and W.W. Hay (2000), Late Cretaceous climate, vegetation, and ocean interactions, in *Warm Climates in Earth's History*, edited by B.T. Huber et al., pp. 275-296, University of Cambridge, Cambridge.

DeConto, R.M. and D. Pollard (2003), Rapid Cenozoic glaciation of Antarctica induced by declining atmospheric CO_2, *Science, 421,* 245-249.

Eagles, G. and R.A. Livermore (2002), Opening history of Powell Basin, Antarctic Peninsula, *Mar. Geol., 185,* 195-205.

Elderfield, H. and M.J. Greaves (1982), The rare earth elements in seawater, *Nature*, *296*, 214-219.

Exon, N.F., J.P. Kennett, M.J. Malone, H. Brinkhuis, G.C.H. Chaproniere, et al. (2001), *Proc. ODP, Init. Repts.,* 189: College Station, TX (Ocean Drilling Program).

Faure, Gunter (1986), *Principles of Isotope Geology*, John Wiley and Sons, New York, pp. 200-216.

Frank, M., N. Whiteley, S. Kasten, J.R. Hein and R.K. O'Nions (2002), North Atlantic Deep Water export to the Southern Ocean over the past 14 Myr: Evidence from Nd and Pb isotopes in ferromanganese crusts, *Paleoceanography, 17*, PA4027, doi:10.1029/2000PA000606.

Grandjean, P., H. Cappetta, A. Michard and F. Albarede (1987), The assessment of REE patterns and $^{143}Nd/^{144}Nd$ ratios in fish remains, *Earth Planet. Sci. Lett., 84,* 181-196.

Goldstein, S.J. and S.B. Jacobsen (1988), Nd and Sr isotopic systems of river water suspended material: implications for crustal evolution, *Earth Planet. Sci. Lett., 87,* 249-265.

Haley, B.A., G.P. Klinkhammer and J. McManus (2004), Rare earth elements in pore waters of marine sediments, *Geochim. Cosmochim. Acta, 68,* 1265-1279.

Halliday, A.N., J.P. Davidson, P. Holden, R.M. Owen and A.M. Olivarez (1992) Metalliferous sediments and the scavenging residence time of Nd near hydrothermal vents, *Geophys. Res. Lett., 19,* 761-764.

Hay, W.W. (1996), Tectonics and climate (review article), in *Global Change and Marine Geology.* Geologische Rundschau, 85, 409-437.

Henderson, G.M. and K.W. Burton (1999), Using $^{234}U/^{238}U$ to assess diffusion rates of isotopic tracers in ferromanganese crusts, *Earth Planet. Sci. Lett., 170,* 169-179.

Houghton, R.L., J.R. Heirtzler, D. Ballard and P.T. Taylor (1977), Submersible observations of the New England Seamounts*, Naturwissenschaften*, 64, 348-355.

Jeandel, C. (1993), Concentration and isotopic composition of Nd in the South Atlantic Ocean, *Earth Planet. Sci. Lett., 117,* 581-591.

Jones, C.E., A.N. Halliday, D.K. Rea and R.M. Owen (1994), Neodymium isotopic variations in the North Pacific modern silicate sediment and the insignificance of detrital REE contributions to seawater, *Earth Planet. Sci. Lett., 127*, 55-66.

Joseph, L.H., D.K. Rea, B.A. van der Pluijm and J.D. Gleason (2002), Antarctic environmental variability since the late Miocene: ODP Site 745, the East Kerguelen sediment drift, *Earth Planet. Sci. Lett., 201,* 127-142.

Katz, M.E. and K.G. Miller (1991), Early Paleogene benthic foraminiferal assemblages and stable isotopes in the Southern Ocean, in: Ciesielski, P. F., Y. Kristofferson et al., pp. 481-512, *Proc. ODP, Sci. Results*, 114: College Station, TX (Ocean Drilling Program).

Lawver, L.A. and L.M Gahagan (2003), Evolution of Cenozoic seaways in the circum-Antarctic region, *Palaeogeog., Palaeoclimatol., Palaeoecol., 198,*11-37.

Ling, H.F., K.W. Burton, R.K. O'Nions, B.S. Kamber, F. von Blanckenburg, A.J. Gibb and J.R. Hein (1997), Evolution of Nd and Pb isotopes in Central Pacific seawater from ferromanganese crusts, *Earth Planet. Sci. Lett., 146,* 1-12.

Lourens, L.J., F.J. Hilgen, J. Laskar, N.J. Schackleton and D. Wilson (2004), The Neogene Period, in *A Geologic Time Scale 2004*, edited by F.M. Gradstein et al., Cambridge University Press, Cambridge.

Michard, A. F. Albarède, G. Michard, J. F. Minster and L.J. Charlou (1983), Rare-earth elements and uranium in high-temperature solutions from East Pacific Rise hydrothermal vent field (13° N), *Nature, 303*, 795-797.

Martin, E.E. and H.D. Scher (2004), Preservation of seawater Sr and Nd isotopes in fossil fish teeth: Bad news and good news, *Earth Planet. Sci. Lett., 220,* 25-39.

Moore, T.C., P.D. Rabinowitz, P.E. Borella, N.J. Shackleton and A. Boersma (1984), History of the Walvis Ridge, in: *Init. Repts., DSDP,* 74, edited by Moore, T.C., Jr., Rabinowitz, P. D., et al., pp. 873-894, U.S. Government Printing Office, Washington, DC.

Nürnberg, D., J. Bijma and C. Hemleben (1996), Assessing the reliability of magnesium in foraminiferal calcite as a proxy for water mass temperatures, *Geochim. Cosmochim. Acta, 60*, 803-814.

O'Nions, R.K., M. Frank, F. von Blanckenburg and H.F. Ling (1998), Secular variation of Nd and Pb isotopes in ferromanganese crusts from the Atlantic, Indian and Pacific Oceans, *Earth Planet. Sci. Lett., 155,* 15-28.

Orsi, A.H., S.S. Jacobs, A.L. Gordon and M. Visbeck (2001), Cooling and ventilating the abyssal ocean, *Geophys. Res. Lett., 28,* 2923-2926.

Orsi, A.H., W.M. Smethie Jr. and J.L. Bullister (2002), On the total input of Antarctic waters to the deep ocean: A preliminary estimate from chlorofluorocarbon measurements, *J. Geophys. Res., 107*(C8), 3101, doi:10.1029/2001JC000976.

Pak, D. K. and K.G. Miller (1992), Paleocene to Eocene benthic foraminiferal isotopes and assemblages: Implications for deepwater circulation, *Paleoceanography,* 7, 405-422.

Palmer, M.R. and H. Elderfield (1986), Rare earth elements and neodymium isotopes in ferromanganese oxide coatings of Cenozoic foraminifera from the Atlantic Ocean, *Geochim. Cosmochim. Acta, 50,* 409-417.

Piepgras, D.J. and G.J. Wasserburg (1984), Strontium and neodymium isotopes in hot springs on the East Pacific Rise and Guaymas Basin, *Earth Planet. Sci. Lett.,* 72, 341-356.

Piepgras, D.J., G.J. Wasserburg and E.J. Dasch (1979), The isotopic composition of Nd in different ocean masses, *Earth Planet. Sci. Lett.,* 45, 223-236.

Piotrowski, A.M., S.L. Goldstein, S.R. Hemming and R.G. Fairbanks (2004), Intensification and variability of ocean thermohaline circulation through the last deglaciation, *Earth Planet. Sci. Lett., 225,* 205-220.

Rabinowitz, P.D. and J. LaBrecque (1979), The Mesozoic South Atlantic Ocean and evolution of its continental margins, *J. Geophys. Res., 84,* 5973-6002.

Reynard, B., C. Lecuyer and P. Grandjean (1999), Chrystal-chemical controls on rare-earth element concentrations in fossil biogenic apatites and implications for paleoenvironmental reconstructions, *Chem. Geol, 155,* 233-241.

Reynolds, B.C., M. Frank and R.K. O'Nions (1999), Nd and Pb-isotope time series from Atlantic ferromanganese crusts: Implications for changes in provenance and paleocirculation over the last 8 Myr, *Earth Planet. Sci. Lett., 173,* 381-396.

Riley, T.R., P.T. Leat, S.P. Kelley, I.L. Millar and M.F. Thirlwall (2003), Thinning of the Antarctic Peninsula lithosphere through the Mesozoic: Evidence from Middle Jurassic basaltic lavas, *Lithos, 67,* 163-179.

Rutberg, R.L., S.R. Hemming and S.L. Goldstein (2000), Reduced North Atlantic deep water flux to the glacial Southern Ocean inferred from neodymium isotope ratios, *Nature, 405*, 935-938.

Salzman, E.S. and E.J. Barron (1982), Deep circulation in the Late Cretaceous: Oxygen isotope paleotempertures from *Inoceramus* remains in DSDP cores, *Palaeogeog., Palaeoclimatol., Palaeoecol., 40,* 167-181.

Savin, S.M. (1977), The history of the Earth's surface temperature during the last 100 million years. *Ann. Rev. of Earth and Planet. Sci., 5,* 319-356.

Scher, H.D. and E.E. Martin (2004), Circulation in the Southern Ocean during the Paleogene inferred from neodymium isotopes, *Earth Planet. Sci. Lett., 228*, 391-405.

Staudigel, H., P. Doyle and A. Zindler (1985), Sr and Nd isotope systematics in fish teeth, *Earth Planet. Sci. Lett., 76,* 45-56.

Stickley, C.E., H. Brinkhuis, S.A. Schellenberg, A. Sluijs, U. Röhl, M. Fuller, M. Grauert, M. Huber, J. Warnaar and G.L. Williams (2004), Timing and nature of the deepening of the Tasmanian Gateway, *Paleoceanography, 19,* PA4027, doi:10.1029/2004PA001022.

Stommel, H. and A. B. Arons (1960), On the abyssal circulation of the world ocean – I. Stationary planetary flow patterns on a sphere, *Deep-Sea Res., 6,* 140-154.

Tachikawa, K., C. Jeandel and M. Roy-Barman (1999), A new approach to the Nd residence time in the ocean: The role of atmospheric inputs, *Earth Planet. Sci. Lett., 170,* 433-446.

Thomas, D.J. (2004), Evidence for deep-water production in the North Pacific Ocean during the Cenozoic warm interval, *Nature, 430,* 65-68.

Thomas, D.J., T.J. Bralower and C.E. Jones (2003), Neodymium isotopic reconstruction of late Paleocene-early Eocene thermohaline circulation, *Earth Planet. Sci. Lett., 209,* 309-322.

Tomczak, M. and J.S. Godfrey (1994), *Regional Oceanography: An Introduction,* Pergamon Press, London.

Vance, D. and K. Burton (1999), Neodymium isotopes in planktonic foraminifera: A record of the response of continental weathering and ocean circulation rates to climate change, *Earth Planet. Sci. Lett., 173*, 365-379.

Vance, D., A E. Scrivner, P. Beney, M. Staubwasser, G. M. Henderson and N. C. Slowey (2004), The use of foraminifera as a record of the past neodymium isotope composition of seawater, *Paleoceanography, 19*, PA2009, doi:10.1029/2003PA000957.

van de Flierdt, T., M. Frank, A.N. Halliday, J.R Hein, B. Hattendorf, D. Günther and P. W. Kubik (2004), Deep and bottom water export from the Southern Ocean to the Pacific over the past 38 million years, *Paleoceanography, 19*, PA1020, doi:10.1029/2003PA000923.

Zachos, J., M. Pagani, L. Sloan, E. Thomas and K. Billups (2001), Trends, rhythms and aberrations in global climate 65 Ma to present. *Science, 27,* 686-693.

Zachos, J., D. Kroon, P. Blum, J. Bowles, P. Gaillot, et al. (2004), *Proc. ODP, Init. Repts.,* 208: College Station TX (Ocean Drilling Program), 1-112.

APPENDIX A

Nd ISOLATION PROCEDURE

I. Cleaning

Fish debris samples were washed twice with ethanol and sonicated, followed by three rinses with 18.2 MΩ Milli-Q (MQ) water. An oxidative solution of 0.1M NaOH and 30% hydrogen peroxide was added to each sample, which were then alternatively warmed and sonicated for 30 minutes. After three MQ rinses, a reductive solution of ammonium hydroxide (NH_4OH), citrate and hydrazine (NH_3NH_3) was added to the samples, followed by another half-hour of alternate warming and sonication. Samples were rinsed three more times with MQ and each sample was dissolved in 200 μL 2M HNO_3 overnight.

II. Separation of REE suite from bulk sample

RE Spec resin in 0.05M HNO_3 was loaded into whole rock columns, cleaned with an aliquot of 0.05M HNO_3 and conditioned with 2M HNO_3. Dissolved samples were added to columns, set with 300 μL 2M HNO_3, rinsed with 3.5 mL 2M HNO_3 and collected with 4.1 mL warm 0.05M HNO_3. Excess liquid was evaporated off by placing on a hot plate. A mixture of 25 μL 2M HCl and 475 μL Milli-Q water was added to each and warmed on a hot plate.

III. Isolation of Nd

Chromatographic separation columns were loaded with BioRad resin in 0.15M α-HIBA acid and cleaned with 200 μL Milli-Q water. The 500 μL aliquot of each sample was added to the columns, followed by another 200 μL Milli-Q water. Samples were the washed first with 4.6 mL 0.15M α-HIBA, then with 2.2 mL 0.225M α-HIBA and finally

collected with 2.7 mL 0.225M α-HIBA. Samples were evaporated on a hot plate, with the addition of aqua regia to purge any remaining resin.

IV. Loading of samples

Dried samples were taken up in 2N HCl and loaded on single rhenium filaments.

VITA

Rachael Kathleen Via received a Bachelor of Science degree in Geological Sciences from the University of North Carolina at Chapel Hill in 2000. She entered the Oceanography Department at Texas A&M University in the Geological Section in August 2003. Her research interests include marine geochemistry, paleoceanography and paleoclimatology. She can be reached at:

Department of Oceanography, College of Geosciences
Texas A&M University
3146 TAMU
College Station, TX 77843-3146
Phone: (979) 845-7211, Fax: (979) 845-6331.